İSTANBUL TECHNICAL UNIVERSITY ★ INSTITUTE OF SCIENCE AND TECHNOLOGY

ELECTROCHEMICAL AND SCANNING PROBE MICROSCOPIC STUDIES ON MODIFIED CARBON FIBER SURFACES

M.Sc. Thesis by
Can Metehan TURHAN, B.Sc.

Department : Polymer Science and Technology
Programme: Polymer Science and Technology

JANUARY 2008

İSTANBUL TECHNICAL UNIVERSITY ★ INSTITUTE OF SCIENCE AND TECHNOLOGY

ELECTROCHEMICAL AND SCANNING PROBE MICROSCOPIC STUDIES ON MODIFIED CARBON FIBER SURFACES

M.Sc. Thesis by
Can Metehan TURHAN B.Sc.
(515051027)

Date of submission: 24 December 2007
Date of defence examination: 30 January 2008

Supervisor (Chairman): Prof. Dr. A. Sezai SARAÇ

Members of the Examining Committee: Prof.Dr. A. Sezai SARAÇ (İ.T.Ü.)

Prof.Dr. Gözen BEREKET (ES.O.G.Ü.)

Assoc. Prof.Dr. Esma SEZER (İ.T.Ü.)

JANUARY 2008

İSTANBUL TEKNİK ÜNİVERSİTESİ ★ FEN BİLİMLERİ ENSTİTÜSÜ

MODİFİYE EDİLMİŞ KARBON FİBER YÜZEYLERİNDE ELEKTROKİMYASAL VE TARAMALI PROP MİKROSKOPİK ÇALIŞMALAR

YÜKSEK LİSANS TEZİ

Can Metehan TURHAN
(515051027)

Tezin Enstitüye Verildiği Tarih : 24 Aralık 2007
Tezin Savunulduğu Tarih : 30 Ocak 2008

Tez Danışmanı : **Prof. Dr. A. Sezai SARAÇ**

Diğer Jüri Üyeleri **Prof.Dr. A. Sezai SARAÇ (İ.T.Ü.)**

Prof.Dr. Gözen BEREKET (ES.O.G.Ü.)

Assoc. Prof.Dr. Esma SEZER (İ.T.Ü.)

OCAK 2008

ACKNOWLEDGEMENT

Firstly, I would like to thank my advisor, Prof. Dr. A. Sezai SARAÇ, for his encouragement, incomparable advices, guidance and discussions in my studies and I have had to learn across broad disciplines, to develop as a scientist.

I would like to express my grateful and sincerest thanks to Prof. Dr. Gözen BEREKET for pushing me to utilize my academic gifts and began to realize my potential at Eskişehir Osmangazi University.

I would like to thank Prof. Dr. Belkıs USTAMEHMETOĞLU, Assoc. Prof. Dr. Esma SEZER, Assoc. Prof. Dr. Deniz HÜR, Dr. Murat ATEŞ, Dr. Elif Altürk PARLAK, Dr. Fevzi Çakmak CEBECİ, Dr. Evrim HÜR for their guidance and advices.

My personal thanks goes to Aslı GENÇTÜRK, Sibel SEZGİN, Koray YILMAZ, Şebnem İNCEOĞLU, N. Ece AYAZ, Bilge KILIÇ and Kerim ÇOBAN for their invaluable advices, patience and friendship during my study.

I would like to thank Dr. Peter van Schendel for precious technical support and advices during AFM measurements and İbrahim İNANÇ for performing SEM measurements with his friendship also acknowledged.

I also want to give my personal thanks to Gamze BAKKALCI, Sezer KÖYLÜ, Berkay YARIZ and Esra ÖZGÜL for their sincerely friendship.

Additionally, I would like to thank my family for precious critics against some of my opinions, respect to my decisions and being always with me at every stage of my life.

And finally, all my praises to the God, from whom all blessings flow.

January 2008 C. Metehan TURHAN

TABLE OF CONTENTS **Page**

LIST OF ABBREVIATIONS

AC	:	Alternating Current
AFM	:	Atomic Force Microscope
ATR-FTIR	:	Attenuated Total Reflectance Fourier Transform Infrared
ACN	:	Acetonitrile
CP	:	Conducting Polymer
CV	:	Cyclic Voltammetry
CF	:	Carbon Fibre
SCFME	:	Single Carbon Fibre Microelectrode
CPE	:	Constant Phase Element
DC	:	Direct Current
EIS	:	Electrochemical Impedance Spectroscopy
EDOT	:	Ethylenedioxythiophene
FE_SEM	:	Field Emmision Scannin Electron Microscopy
HOMO	:	Highly Oriented Molecular Orbitals
IHP	:	Inner Helmholtz Plane
IRE	:	İnternal Reflectance Element
ITO	:	İndium Tin Oxide
MO	:	Molecular Orbital
$NaClO_4$	:	Sodiumperchlorate
PA	:	Polyacetylene
PAN	:	Polyacrylonitrile
PPS	:	Poly(phenylenesulfide)
PEDOT	:	Poly(3,4-ethylenedioxythiophene)
$PProDOT\text{-}Bu_2$	:	Poly(2,2-Dimethyl-3,4-propylenedioxythiophene)
R	:	Alkyl group
SEM	:	Scanning Electron Microscope

LIST OF SYMBOLS

C_{sp}	: Specific Capacitance
C_{dl}	: Double Layer Capacitance
E_g	: Band Gap
E_{eq}	: Equivalant Potential
$E_{1/2}$	: Half wave potential
$E_{a,\ c}$	: Oxidation, Reduction Potential
E_{onset}	: Onset potential
$I_{a,\ c}$	: Anodic, Catodic Peak Current
Q_{pg}	: Deposition Charge
R_p	: Polarization Resistor
I	: Current
ν	: Scan rate
λ	: Wavelength
A	: Absorbance
E_{pa}, E_{pc}	: Anodic and catodic oxidizing and reducing potential
t	: Time
M	: Molarity
%T	: Percantage transparency
Q	: Charge
Q_{dep}	: Deposition charge
F	: Faraday constant
A	: Electrode area

LIST OF TABLES

LIST OF FIGURES

ELECTROCHEMICAL AND SCANNING PROBE MICROSCOPIC STUDIES ON MODIFIED CARBON FIBER SURFACES

SUMMARY

In 1976, electrical conductivity in a conjugated polymer (polyacetylene) was reported by Shirakawa, Heeger and MacDiarmird [1]. After that, combining these new conjugated materials with the properties of organic polymers has been studied for various applications.

The preparation, characterization and application of conducting polymers are still mostly research activity in the electrochemistry. Electrochemical polymerization represents a widely employed route for the synthesis of some important classes of conjugated polymer such as thiophene (Th).

Carbon fiber is made from graphite which is a form of pure carbon. In graphite, the carbon atoms are arranged into big sheets of aromatic ring and porous carbon is the most frequently selected electrode material which offers a large surface area. Due to porosity, carbon is one of the most promising electrode material for supercapacitor application.

Carbon fiber micro electrodes shows superior performance in electrochemical studies due to their micron size and cylindrical structure. Its disposable character having a new surface area at each time rather than Pt or ITO electrodes. For many cases carbon fiber electrodes reveals better reversibilities than the other electrodes.

Poly (3,4- alkylenedioxythiophene)s (PXDOTs), have attracted attention across academia and industry with their special polymerizaiton routes. Due to their ability to be functionalized at the 2-position of the propylene bridge, ProDOT (Pro=1,3-propylene) monomers and polymers have gained special interest as the polymers that form are regio-symmetric.

By increasing the ring size from dioxane (six-membered) to the seven-memnered ring in ProDOT, little change is seen in the electropolymerization and switching behavior of PProDOT relative to PEDOT.

Electropolymerization process was performed in 0.1M $NaClO_4$ in ACN at various cycle numbers with a constant monomer concentration of 10^{-2} M.

Electrochemical Impedance Spectroscopy (EIS) measurements were performed at both open circuit potential in the range of 0.1V -1.4 V between 100 kHz - 10 mHz (excitation of amplitude of 10 mV).

$PProDOT(Bu)_2$ electrochemically obtained at different charges (cycles), and at different applied potentials in the range of -0.1 V to 1.3 V with a potential step of 0.1V.

In parallel to cyclic voltammogram of the PProDOT-Bu_2 in monomer free electrolyte solution, the stability of the film exhibit electroactivity without undergoing deformation up to 0.8 V.

The shape of the electrogrowth plot has a very good agreement with the corresponding CV of the polymer film in monomer free solution. The low capacitance values increase in low potentials, at 0.4 V capacitance values shows a maximum point which converges very well at this potential observed in CV of the ProDOT-Bu_2 film for 100 mV/s.

The electrochemical parameters of the SCFME/P(ProDOT-Bu_2) in $NaClO_4$ system was evaluated by employing the ZSimpWin (version 3.10) software from Princeton Applied Research. Equivalent electrical circuit model and variation of the solution resistance, double layer capacitance and low frequency capacitance of the PProDOT-Bu_2 films with several cycles were investigated in this study.

AFM is an essential tool to observe identificial characteristics of film morphologies with three dimensional images. In this study non-contact mode was employed with high frequency silicon tips with Al coating.

Morphology of coatings for different applied charge densities and different applied potentials were studied. The SEM pictures show a pronounced difference in the surface morphology of the two type of different P(ProDOT-Bu_2) layers with increasing cycle number.

In the beginning, after very thin film formation on SCFME, where striations sligthly disappear on the whole surface area, a polymeric layer appears with nano-size villus like structures were obtained after 20 cycles.

At applied potentials afte 0.8 V, the film morphology changed and capacitance of modified electrodes decreased.

Finally, investigation of out different substares such as Pt, ITO coated glass showed that SCFMEs are the most suitable ones for using supercapacitor components in comparasion with other 10 cycle coated Pt and ITO electrodes.

MODİFİYE EDİLMİŞ KARBON FİBER YÜZEYLERİNDE ELEKTROKİMYASAL VE TARAMALI PROP MİKROSKOPİK ÇALIŞMALAR

ÖZET

1976'de Alan MacDiarmid, Hideki Shirakawa ve bir grup araştırmacı iletken polimerleri keşfetti. Diğer iletken polimerlerin sentezi, bu keşiften sonra araştırmacılar tarafından büyük ilgi uyandırmıştır. İletken polimer filmlerde elektriksel iletkenlik, anyonik ve katyonik türlerin yüklenmiş olarak yapıya girmesini takip eden yükseltgenme (p-katkılandırma) ve indirgenme (n-katkılandurma) yolu ile gerçekleşmekte ve konjuge polimerlerin anazincirlerindeki çift bağların değişmesi ile katkılandırmadan oluşan yüklenmiş türler yardımıyla karbon zinciri boyunca elektronun taşınması, malzemeye iletkenlik kazandırır.

İletken polimerlerin sentezi kimyasal ve elektrokimyasal olmak üzere ikiye ayrılır. Elektrokimyasal polimerizasyon genellikle döngülü voltamogram kullanılarak anodik oksidasyon ile çalışma elektrodunun üzerinde gerçekleştirilir. Son dönemlerde çalışma elektrotları karbon bazlı yapılar arasından seçilmektedir.

Karbon fiber bir çeşit grafit formu olarak tanımlanırken, grafit ise saf karbon olarak adlandırılabilir. Grafit yapısında karbon atomları düzlemsel yapı üzerinde bulunan hekzagonal halkalar şeklindedir.

Porlu bir yapıya sahip olan karbon, bunun yanında geniş yüzey alanı sağlama ve iyi polarize olması açısından süper kapasitör uygulamalarında tercih edilen bir malzemedir. Bunun yanında, birçok durumda metal elektrotlara nazaran daha iyi sonuçlar verdikleri saptanmıştır.

Yüksek ve kararlı iletkenlik sergileyen iletken ve elektroaktif polimerler sınıfına giren poli (3,4-alkilendioksitiyofen)'ler (PXDOT), propilen köprüsünün ikinci pozisyonun fonksiyonlanmasının getirdiği özellikten dolayı özel bir ilgi çekmektedirler.

ProDOT (Pro=1,3-propilen) monomeri ve polimeri halka büyüklüğünün altı üyeliden yedi üyeliye artması elektrokaplamada ve spektroelektrokimyada PEDOT polimerine göre küçük değişiklik gösterir.

Bu çalışmada ProDOT-Bu_2 monomerleri döngülü voltametri ile KFME üzerine kaplanmış, polimerlerin karakterizasyonu ve elektriksel impedans özellikleri araştırılmıştır.

Elektrokaplama 0-1.6 V 'da, 100 mVs^{-1} tarama hızında, 0.1 M $NaClO_4$/ACN içerisinde TKFME (Tek karbon fiber mikroelektrot) üzerine döngülü voltametri ve değişik döngülerde gerçekleştirilmiştir.

Elektrokimyasal empedans ölçümleri 100 kHz - 10 mHz aralığında hem açık devre potansiyelinde döngü sayısı göz önüne alınarak, hem de farklı potansiyeller uygulanarak (20 döngü için) gerçekleştirilmiştir (0.1 V artan potansiyel aralıklarla 0.1 V'dan 1.4 V'a farklı potansiyellerde).

Ayrıca, empedans ölçümleri farklı döngüler için de incelenmiş ve film kalınlığının artışının kapasitif özelliklere yansıması incelenmiştir.

Elde edilen kapasitans değerlerin, polimerin döngülü voltametri grafiğine benzediği görülmüştür. Ayrıca elde edilen ince filmin en kapasitif davranışı 0.4 V' ta gösterdiği ve 0.8 V' tan sonra kapasitif davranışının film yapısına parallel olarak değiştiği saptanmıştır.

KFME/PProDOT-Bu_2/Elektrolit sisteminde elektrokimyasal parametreler Princeton Applied Research cihazı için uygulanan ZSimpWin (versiyon 3.10) yazılımında modellenmiştir. PProDOT-Bu_2 filminin çözelti direncinin çeşitliliği, çift tabaka kapasitans ve düşük frekans kapasitans değerleri hem farklı döngüler hem de uygulanan farklı potansiyeller için denemiştir. Sonuçlar karşılaştırılarak önerilen eşdeğer devrenin bileşenler elde edilen sonuçların belirli bir artma ve belirli bir azalma içinde olmalarından ötürü açıklanmıştır.

Üç boyutlu görüntü vermesinden dolayı, atomik kuvvet mikroskobu önemli bir cihazdır. Bu çalışmada da yüzey üzerindeki filmin oluşumu atomik kuvvet mikroskobu ve taramalı elektron mikroskobu ile incelenmiş ve sonuçlar karşılaştırılmıştır.

Polimerizasyonun birinci, üçüncü ve beşinci döngülerinde TKFME üzerinde yoğunlaşmaya başlayan tanecikler, özellikle onuncu döngüden sonra yoğunlaşmaya başlamışlar ve yirminci döngüde nano-vilus benzeri yapılar sergilemişlerdir.

Elde edilen yüzey resimlerinden, 0.8 V potansiyel uygulanmasından sonra yüzeyin değiştiği ve nano-vilus benzeri yapıların ortadan kalktığı gözlemlenmiştir.

Son olarak polimerizasyon farklı yüzeylerde de gerçekleştirilmiş (Platin ve indiyum kalay oksit kaplı cam) ve sonuçlar KFME'lar ile karşılaştırılmıştır. Elde edilen sonuçlar KFME'ların kapasitif özellikler amacında daha üstün olduklarını göstermektedir.

1. INTRODUCTION

1.1 Conductive Polymers

Electrical conductivity was reported in 1977 [1] by Shirakawa, Heeger and MacDiarmird for a conjugated polymer, and the research on conducting polymers have been continuous for several years. Many researchers have been focused on the conducting polymers to commercialize them with applications [2-6].

In 1958, polyacetylene was first synthesised by Natta as a black powder. This was found to be a semi-conductor with a conductivity between $7x10^{-11}$ to $7x10^{-3}$ S m^{-1}, depending upon how the polymer was processed and manipulated. This compound remained a scientific curiosity until 1967, when a postgraduate student of Hideki Shirakawa at the Tokyo Institute of Technology was attempting to synthesize polyacetylene, and a silvery thin film was produced as a result of a mistake. It was found that 1000 times too much of the Ziegler-Natta catalyst, $Ti(O\text{-}n\text{-}But)_4$ - Et_3Al, had been used. When this film was investigated it was found to be semiconducting, with a similar level of conductivity to the best of the conducting black powders. Further investigations, initially aimed to produce thin films of graphite, showed that exposure of this form of polyacetylene to halogens increased its conductivity a billion fold. Undoped, the polymer was silvery, insoluble and intractable, with a conductivity similar to that of semiconductors. When it was weakly oxidized by compounds such as iodine it turned a golden colour and its conductivity increased to about 104 S m^{-1}. The possibility of combining in these new materials the properties of organic polymers and the electronic properties of semiconductors has been the driving force for various applications.

Electronically conducting polymers, such as polypyrrole, polythiophene or polyaniline, are a class of organic semiconductors with many possible areas of application [7].

Conducting polymers (CPs) are an exciting new class of electronic materials, which have attracted rapidly increasing interest since their discovery in 1979.

CPs have the potential of combining the high conductivities of pure metals with the processibility, corrosion resistance and low density of polymers [8] and are beginning to find applications in the fields of battery materials [9], electrochromic displays [10], electromagnetic shielding [11], sensor technology [12], non-linear optics [13] and molecular electronics [14-15].

Films of electronically conducting polymers are generally obtained onto a support electrode surface by anodic oxidation (electropolymerization) of the corresponding monomer in the presence of an electrolyte solution. Different electrochemical techniques can be used including potentiostatic (constant potential), galvanostatic (constant current), and potentiodynamic (potential scanning i.e. cyclic voltammetry) methods. Electrically conductivity is achieved in the film of conducting polymer by oxidation (p-doping) or reduction (n-doping), followed respectively by the insertion of anionic or cationic species [16]. The π-electron system along the polymer backbone, which confers rigidity and the cross linking points between polymer chains, make conducting polymers insoluble, infusible and poorly processable.

During the last twenty years, conjugated polymers, such as polyacetylene, polyaniline, polypyrrole, polythiophene, etc., have attracted tremendous attention, mainly because of their interesting optical, electrochemical and electrical properties (Figure 1.1). These properties may lead to variety of applications such as information storage, electroluminescent devices, optical signal processing, solar energy conversion materials, electrochemical cells, EIM shielding, antistatic coatings, bioelectronic devices, etc. [17-20]. For instance, these materials are well known for their high electrical conductivity arising upon doping (oxidation, reduction and protonation). The delocalized electronic structure of these polymers is partly responsible for the stabilization of the charge carriers created upon doping and electrical conductivities in the range of 1-1000 S cm^{-1} can be reached in most cases. Moreover, processibility and a high level of conjugation have been obtained through the incorporation of alkyl side chains on polythiophene [21-26].

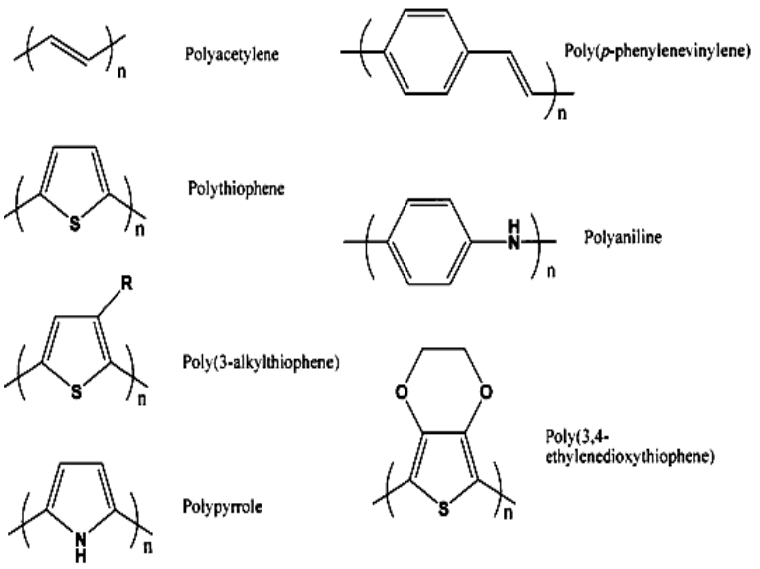

Figure 1.1: Molecular Structures of Several Conjugated Polymers.

1.1.1 Electrical Conductivity and Band Gap Theory

The electrical properties of any material are a result of the material's electronic structure that CP's form bands through extensive molecular orbital overlap leads to the assumption that their electronic properties can be explained by band theory. In this theory materials are classified as metals, semiconductors, or insulators indicated in Figure 1.2.

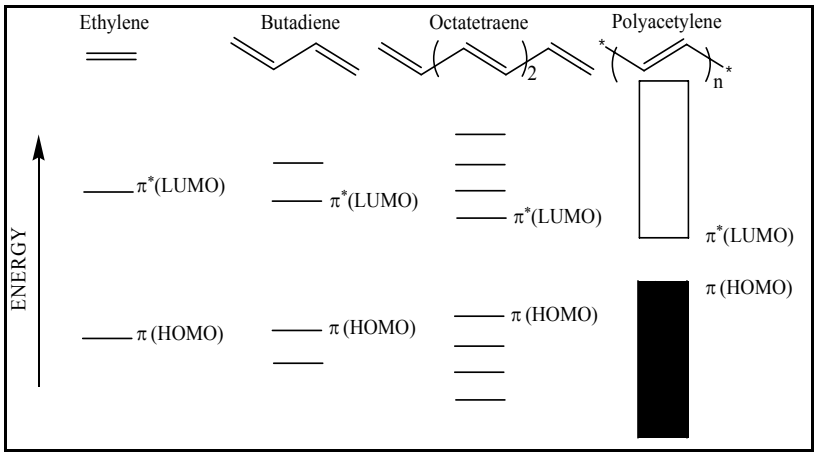

Figure 1.2: Molecular orbital (MO) diagram.

There is enough energy separation between the conduction and valence bands that thermal energy alone is insufficient to excite electrons across the band gap.

For electrical conductivity to occur, an electron must have a vacant place to move and occupy. When bands are completely filled or empty, conduction can not occur. Metals are highly conductive because they have unfilled bands.

Semiconductors have an energy gap small enough that thermal excitation of electrons from the valence to the conduction bands is sufficient for conductivity; however, the band gap in insulators is too large for thermal excitation of an electron across the band gap (Figure 1.3).

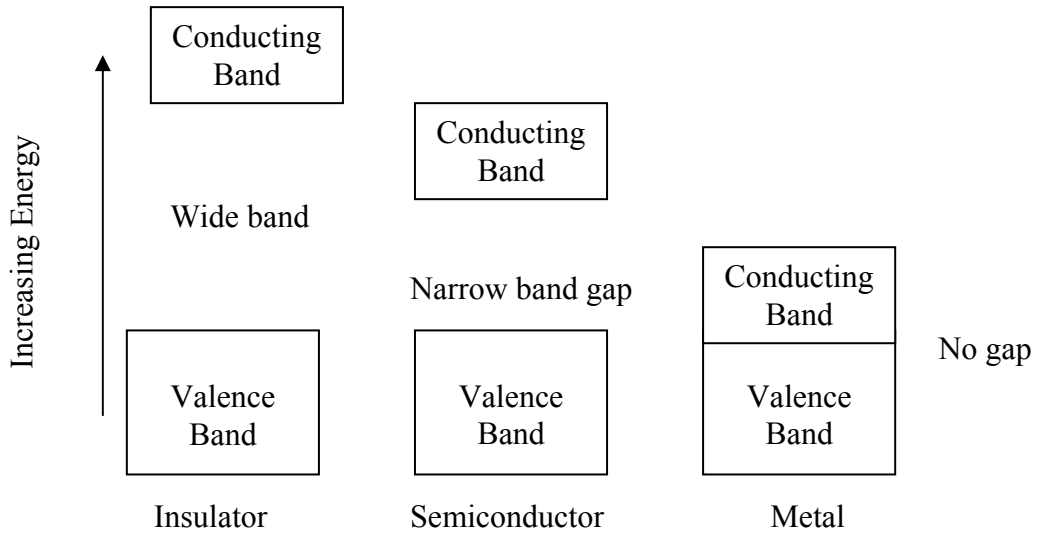

Figure 1.3: Classification of materials and schematic of valence and conduction.

1.1.2 Doping Process and Polaron-Bipolaron Structures

The electrochemical switching of a conducting polymer (CP) between the doped and undoped states involves both electron and ion injection into or extraction from the polymer, concomitant with the transport of electronic and ionic charges within the CP. Consequently, the charge transport processes inside the CP bulk, as well as across the CP's interfaces, constitute crucial points in many applications and have been the object of extensive researches.

In particular, it has been reported that in most cases ion transport is the slow process, i.e. the step limiting the switching rates of, for example, displays and electronic devices based on similar materials [27].

The main criteria is its ability to oxidize or reduce the polymer without lowering its stability or whether or not they are capable of initiating side reactions that inhibit the polymers ability to conduct electricity.

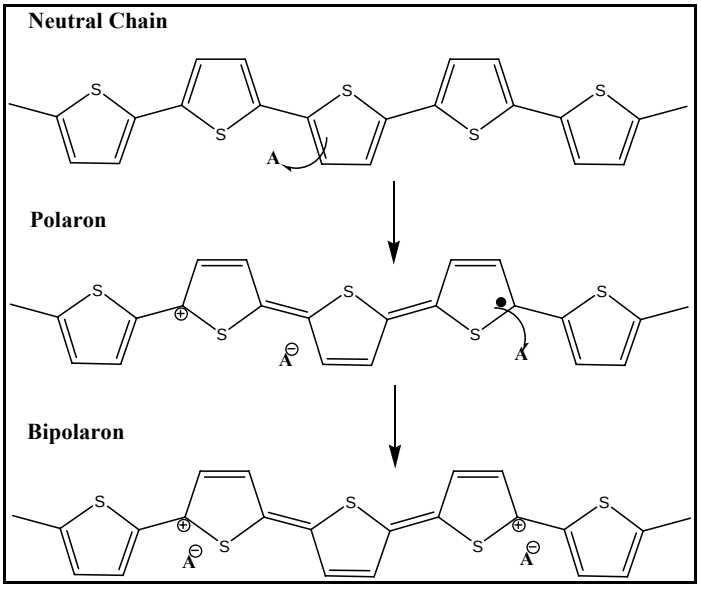

Figure 1.4: Oxidative doping of thiophene ($A^{\ominus}$: dopant).

The oxidative doping of polythiophene proceeds in the following way Figure 1.4. An electron is removed from the π-system of the backbone producing free radical and a spinless positive charge. The radical and cation are coupled to each other via local resonance of the charge and the radical.

Upon further oxidation the free radical of the polaron is removed, creating a new spinless defect called a bipolaron. This is of lower energy than the creation of two distinct polarons. At higher doping levels it becomes possible that two polarons combine to form a bipolaron. Thus at higher doping levels the polarons are replaced with bipolarons. This eventually, with continued doping, forms into a continuous bipolaron bands [28].

1.1.3 Polyalkylenedioxythiophenes

Due to its high oxidation potential, thiophene itself is difficult to polymerize electrochemically. The best results are obtained in BF_3-Et_2O medium [29]. However, upon alkyl substitution the monomer oxidation potential is lowered to an easily accessible range, which has resulted in the extensive study of poly(3-methyl thiophene) and other poly(3-alkylthiophenes) [30].

Substitution at the 3- and 4- positions of thiophene prevents the occurrence of α-β and β - β coupling during electropolymerization, yielding more ordered polymers with longer conjugation lengths.

Initially, the synthesis of 3,4-disubstituted polythiophenes were carried out with the goal of stabilizing the oxidized form as well as providing solubility and processibility [31]. While these substituents do lower the oxidation potential and stabilize form of the polymers to nucleophilic attack, they also lead to severe steric interactions that distort π conjugated system [32], decreasing the degree of conjugation and lowering the conductivity.

To overcome this drawback, poly(3-4-cycloalkylthiophenes) [33] were synthesized, and it was demonstrated that carbocycles at at the 3- and 4- positions reduced the steric hinderence, especially in the case of poly(3,4-cyclopentylthiophene). This strategy was taken a step further and the methylene adjacent to the heterocycle was replaced by an heteroatom such as oxygen [34,35], making the oxidized form form even more stable with less steric distortion. As a result, polythiophenes carrying 3,4-dialkoxy and 3,4-alkylenedioxy substituents exhibit the most pronounced stability.

Jonas et al. [36] were the first to anodically polymerize a member of the 3,4-alkylenedioxythiophene family, 3-4-ethylenedioxythiophene. It was found that the resulting poly(3,4-ethylenedioxythiophene) was highly conducting and more stable than other polythiophenes.

To date, a large family of poly(3,4-alkylenedioxythiophene)s (PXDOTs) (Figure 1.5) has been synthesized to elucidate the structure-property relationship in these materials.

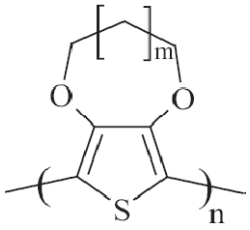

Figure 1.5: Poly (3, 4- alkylenedioxythiophene)s (PXDOTs).

As a class of conducting and electroactive polymers that can exhibit high and quite stable conductivities, a high degree of optical transparency as a conductor, and the ability to be rapidly switched between conducting doped and insulating neutral states, poly (3,4- alkylenedioxythiophene)s (PXDOTs), have attracted attention across academia and industry.

Since both chemically and electrochemically prepared PXDOT is insoluble and unprocessible, intensive research has been carried out to synthesize PXDOT derivatives that would overcome this problem.

Due to their ability to be functionalized at the 2-position of the propylene bridge, ProDOT (Pro=1,3-propylene) monomers and polymers have gained special interest as the polymers that form are regio-symmetric. By increasing the ring size from dioxane (six-membered) to the seven-membered ring in ProDOT, little change is seen in the electropolymerization and switching behavior of PProDOT relative to PEDOT. There are distinct changes in the physical properties of the monomers as EDOT is a liquid at room temperature, while ProDOT is a solid. This makes purification by recrystallization and access to highly pure ProDOT monomers quite facile. There are large changes observed when comparing the optical properties of the substitued PProDOTs, especially the dimethyl and diethyl derivatives that exhibit enhanced electrochromic contrasts throughout the visible region [37]. This will be addressed further later. In addition, by appending long chains at the 2-position of the propylene bridge, soluble and peocessible PProDots are accessible, which are not only electroactive but are also highly fluorescent (deep-red emission) in solution [38].

Turning to the eight-membered ring-containing species. BuDOT (Bu=butylene), again little change is observed in electropolymerizability and switching relative to PEDOT or PProDOT. It should be noted that pentylene functionallized derivative, which might gain the acronym PenDOT, has not been synthesized to date due to the difficulty in closing nine-membered rings, and remains elusive [39].

1.1.4 Supercapacitors

Conventional capacitors consist of two conducting electrodes separated by an insulating dielectric material. When a voltage is applied to a capacitor, opposite charges accumulate on the surfaces of each electrode.

The charges are kept separate by the dielectric, thus producing an electric field that allows the capacitor to store energy. This is illustrated in Figure 1.6.

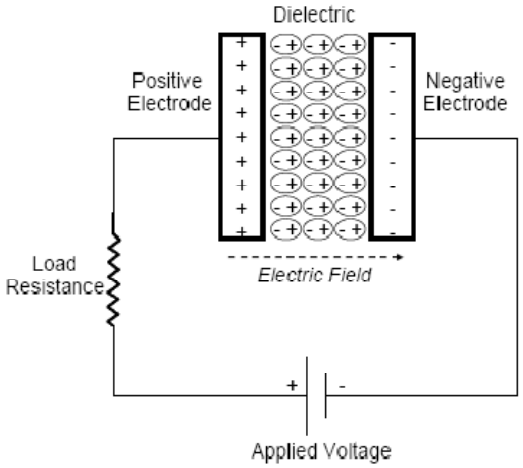

Figure 1.6: Schematic of a conventional capacitor.

Capacitance C is defined as the ratio of stored (positive) charge Q to the applied voltage V:

$$C = Q/V \quad \textbf{(1.1)}$$

For a conventional capacitor, C is directly proportional to the surface area A of each electrode and inversely proportional to the distance D between the electrodes:

$$C = \varepsilon_0 \varepsilon_R A/D \quad \textbf{(1.2)}$$

The product of the first two factors on the right hand side of the last equation is a constant of proportionality wherein ε_0 is the dielectric constant (or "permittivity") of free space and ε_R is the dielectric constant of the insulating material between the electrodes.

The two primary attributes of a capacitor are its energy density and power density. For either measure, the density can be calculated as a quantity per unit mass or per unit volume. The energy E stored in a capacitor is directly proportional to its capacitance:

$$E = 1/2\ CV^2 \quad \textbf{(1.3)}$$

In general, the power P is the energy expended per unit time. To determine P for a capacitor, though, it should be considered that capacitors are generally represented as a circuit in series with an external "load" resistance R, as is shown in Figure 1.6.

The internal components of the capacitor (e.g., current collectors, electrodes, and dielectric material) also contribute to the resistance, which is measured in aggregate by a V quantity known as the equivalent series resistance (ESR). The voltage during discharge V is determined by these resistances. When measured at matched impedance (R = ESR),V the maximum power P_{max} for a capacitor [40-42] is given by:

$$P_{max} : V^2 / (4xESR) \quad \textbf{(1.4)}$$

This relationship shows how the ESR can limit the maximum power of a capacitor.

Conventional capacitors have relatively high power densities, but relatively low energy densities when compared to electrochemical batteries and to fuel cells. That is, a battery can store more total energy than a capacitor, but it cannot deliver it very quickly, which means its power density is low. Capacitors, on the other hand, store relatively less energy per unit mass or volume, but what electrical energy they do store can be discharged rapidly to produce a lot of power, so their power density is usually high.

Supercapacitors are governed by the same basic principles as conventional capacitors. However, they incorporate electrodes with much higher surface areas (A) and much thinner dielectrics that decrease the distance (D) between the electrodes. Thus, from (1.2) and (1.3), this leads to an increase in both capacitance and energy.

Furthermore, by maintaining the low ESR characteristic of conventional capacitors, supercapacitors also are able to achieve comparable power densities.

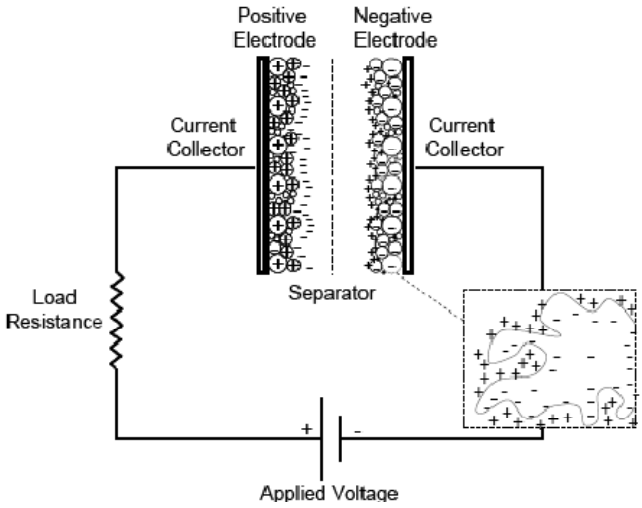

Figure 1.7: Schematic of a double layer capacitor.

Additionally, supercapacitors have several advantages over electrochemical batteries and fuel cells, including higher power density, shorter charging times, and longer cycle life and shelf life. Figure 1.7 provides a schematic diagram of a supercapacitor, illustrating some of the physical features described above.

Supercapacitors, also known as ultracapacitors or electrochemical capacitors, utilize high surface area electrode materials and thin electrolytic dielectrics to achieve capacitances several orders of magnitude larger than conventional capacitors.

Performance of a supercapacitor (or ultracapacitor) combines simultaneously two kinds of energy storage i.e. an electrostatic attraction as in electric double layer capacitors (EDLC) and faradaic reactions similar to processes proceeding in accumulators. Pseudocapacitance arises when, for thermodyamic reasons, the charge q required for the progression of an electrochemical process is a continously changing function of potential U. Then the derivative C=dq/dU corresponds to a faradaic kind of capacitance.

The term *pseudo* originates from the fact that the double layer capacitance arises from quick faradaic charge transfer reactions and not only from electrostatic charging. An ideal double layer capacitance behavior of an electrode material is expressed in the form of a rectangular shape of the voltametry characterictic behavior of supercapacitors. In this type of energy storage, the phenomenon is purely electrostatic and current is independent on potential.

On the other hand, electrode materials with pseudocapacitance properties point out a deviation from such a rectangular shape and reversible redox peaks connected with pseudofaradaic reactions are remarkable. In this case charge accumulated in the capacitor is strongly dependent on the electrode material. This observed delay of potential during reversing the potential sweep is related with a kinetically slow process involved during charging pseudocapacitance.

Contrarily, in the electrochemical capacitors, the electrical charge is accumulated in the double layer mainly by electrostatic forces without phase transformation in the electrode materials.

The stored electrical energy is based on the separation of charged species in an electrical double layer across the electrode / solution interface (Figure 1.8).

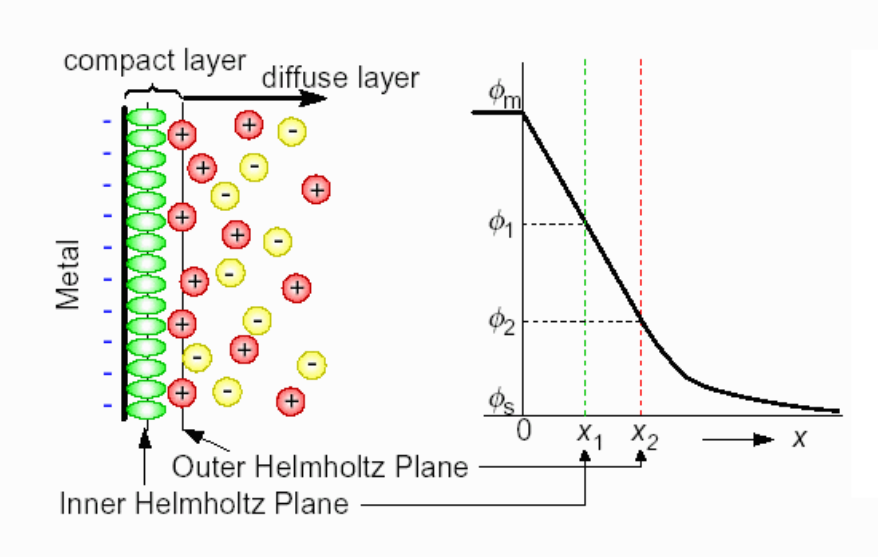

Figure 1.8: Scheme of the Electrochemical Double Layer.

The maximal charge density is accumulated at the distance of outer Helmholtz plane, i.e. at the centre of electrostatically attracted solvated ions. The electrochemical capacitor contains one positive electrode with electron deficiency and the second one negative with electron excess, both electrodes being built from the same material. The amount of electrical energy W accumulated in such capacitors is proportional to capacitance C and voltage U according to the formula:

$$W=1/2CU^2 \qquad \textbf{(1.5)}$$

The electrochemical withdrawing of energy from these two types of power sources differs significantly.

It is clear that in a typical accumulator a charge/ discharge plateau is observed for the dependence $U = f(t)$, and for an electrochemical capacitor we have almost a linear decay of voltage with time. As a consequence, the energy stored in the capacitor ($1/2\ qU$) is half that for the equivalent battery cell (qU) [43].

1.2 Electropolymerization

Electrochemical polymerization is recognized as an effective technique for the synthesis of conducting polymers. It is widely used, because it is simple and can be used as a one step method [44].

The electropolymerization procedure offers the advantage of controlling the thickness, and functionality of such a 'reactive' coating through selective process parameters (i.e. current density and monomer concentration, etc.) and uniform coatings can be achieved [45].

At the beginning of the electrochemical reaction the monomer, dissolved in an appropriate solvent containing the desired anionic doping salt, is oxidized at the surface of an electrode by application of an anodic potential (oxidation). The anode can be made of a variety of materials including platinum, carbon fiber, gold, glassy carbon, and tin or indium-tin oxide (ITO) coated glass.

During the process, the monomer is electrochemically oxidized at a polymerization potential giving rise to free radicals.

These radicals are adsorbed onto the electrode surface and undergo subsequently a wide variety of reactions leading to the polymer network [46]. As a result of the initial oxidation, the radical cation of the monomer is formed and reacts with other monomers present in solution to form oligomeric products and then the polymer.

The extended conjugation in the polymer results in a lowering of the oxidation potential compared to the monomer. Therefore, the synthesis and doping of the polymer are generally done simultaneously.

In Figure 1.9, electrochemical polymerization mechanism of heterocyclic compounds is shown. The growth of this polymer depends on its electrical character. If the polymer is electrically nonconducting, its growth is self-limited.

Such films are very thin (10 - 100 nm). In contrast, the growth of conductive polymers is virtually unlimited.

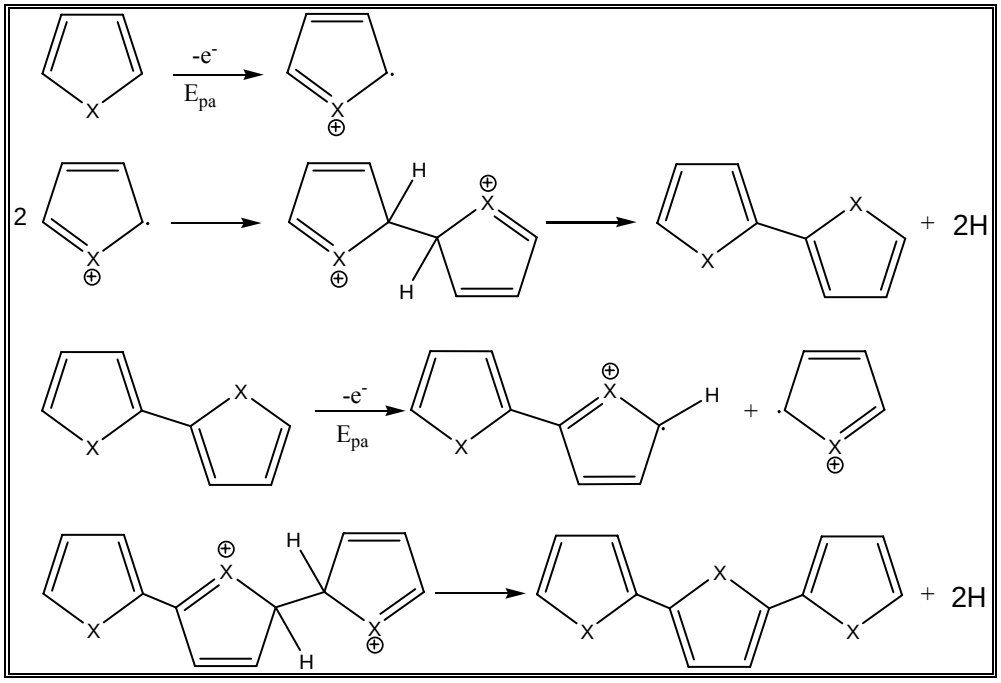

Figure 1.9: Electropolymerization pathway for valid heterocyclic compounds.

The process is governed by the electrode potential and by the reaction time, which allows to control the thickness of the resulting film. In order to have uniform and reproducible results, the process parameters of electrochemical polymerization have to be optimized. The parameters; type of electrolyte, concentration ratio of monomer and electrolyte, pH of the electrolyte, monomer substitution, scan rate, solvent, temperature and current density affect the conductivity and morphology of the synthesized polymer film.

There are mainly 3 types of electropolymerization techniques. These are:

1. Potentiodynamic by cyclic voltammetry
2. Choronoamperometry (constant potential)
3. Choronopotentiometry (constant current)

These techniques are easier to describe quantitatively and have been therefore commonly utilized to investigate the nucleation mechanism and the macroscopic growth.

Voltammetry uses four major types of excitation signals in order to vary the potential: linear scan, differential pulse, square wave, and triangular (Figure 1.10). Each variable potential excitation signal is applied to the electrochemical cell containing a microelectrode over time and induces a characteristic current response.

Linear and triangular excitation signals vary the potential applied to the working electrode linearly over time (Figure 1.10; (a) and (d)). When triangular excitation signals are used, we call the voltammetric method cyclic voltammetry. Pulsed voltammetric methods include differential pulse and square wave excitation signals, which vary the potential differently over time (Figure 1.10; (b) and (c)) and are of great analytical use because they minimize the interference of capacitive or nonfaradaic currents.

A current that is due to electrolysis is a faradaic current and isthe useful current in pulsed voltammetric methods. Changing the potential applied to an electrode contributes a second current, called a nonfaradaic current, to the overall observed current, where the total current measured is the sum of the faradaic and nonfaradaic currents.

As the potential is changed, the electrode must be charged resulting in a nonfaradaic current. Advances in voltammetry have led to improvements in the sensitivity of pulsed voltammetric methods, allowing interfering nonfaradaic currents to be separated from analytically useful faradaic currents. The manipulation of the voltage applied to the working electrode provides three useful types of voltammetry; cyclic voltammetry, square wave voltammetry, and differential pulse voltammetry.

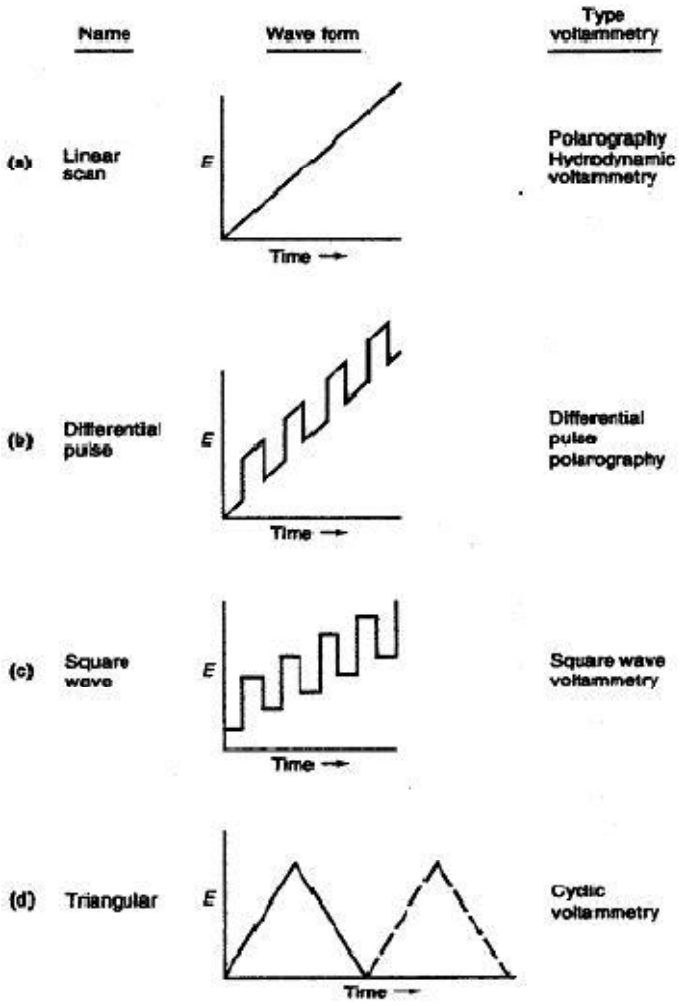

Figure 1.10: Four Types of Voltammetric Signals.

1.2.1 Cyclic Voltammetry

In cyclic voltammetry (CV), a triangular wave form (Figure 1.10; (d)) is used to vary the potential applied to the working electrode linearly in both the forward and reverse direction. Because of the large overpotential of mercury electrodes, CV scans in natural waters are typically run from –0.1V to –1.8V and back to –0.1V (I-F-I scans) so that reversible electrochemical reactions can be detected. The rate at which the potential is changed (voltage / time) is called the scan rate. The potential range used when running a CV scan depends on the type of working electrode and the electrolyte it is in.

As the varying potential is applied to the working electrode, the current is recorded. An advantage of CV over linear sweep voltammetry is the ability to determine if an electrochemical reaction is reversible by comparing the forward (cathodic) and reverse (anodic) peak currents and peak potentials. If a reaction is truly reversible the peak separation between the cathodic peak potential and the anodic peak potential will be 0.0592 V/ electron.

1.2.2 Square Wave Voltammetry

In square wave voltammetry (SWV), the square wave form (Figure 1.10; (c)) consists of a symmetrical square wave pulse of the potential applied to the working electrode, where the amplitude and step height can be defined by the user. The result of the staircase waveform is a forward pulse that produces a cathodic current and a reverse pulse that produces an anodic current.

The net current, or resultant current, is the difference between the forward and reverse currents and is centered on the base potential of the wave pulse. Current peak heights, from the resultant current, are directly proportional to the concentration of the electroactive species reduced at the working electrode. Advantages to SWV include its excellent sensitivity, rejection of background currents, and the fast speeds at which scans can be run.

1.2.3 Differential Pulse Voltammetry

Differential pulse polarography (DPP) uses the differential pulse excitation signal (Figure 1.10; (b)) where a series of small pulses are made to the potential applied to the working electrode. Each potential pulse is fixed, has a small amplitude, and is superimposed on a slowly changing base potential. In order to separate the faradaic and nonfaradaic currents, the total current is measured twice; once just prior to the voltage pulse providing a baseline current, and once close to the end of the pulse when the nonfaradaic currents have decreased significantly.

The difference between the two currents at each pulse, the resultant current, is determined and centered on the base potential of the pulse. DPP has two major advantages, the ability to separate peaks at similar potentials and excellent sensitivity.

1.2.4 Stripping Voltammetry

Stripping voltammetry involves the pre-concentration of an analyte on the surface of the working electrode before running a voltammetric scan. Pre-concentrating an analyte on the surface of the working electrode can be accomplished by applying a potential to the working electrode for a certain amount of time.

Certain analytes in solution are able to react with the surface of the electrode forming an amalgam that can then be measured or stripped from the electrode by running a potential scan (CV, SWV, DPP).

The amount of time the potential is held during the pre-concentration step, while consistently stirring the solution, directly affects the sensitivity of the electrochemical method, lowering the detection limits of certain analytes.

1.2.5 In Situ Voltammetry

Voltammetric techniques can be applied to environments where redox chemistry needs to be defined *in situ*. The ability to detect and measure multiple chemical species in the same potential scan makes voltammetric techniques useful for investigating redox chemistry. Several electrode systems, based on voltammetric methods, have been designed for *in situ* detection of chemical species of oxygen, sulfur, iron, manganese, iodide, and many trace metals.

Working electrodes designed for these systems make it possible to detect particular chemical species; however, they are not able to detect metals and redox species important to anaerobic oxidation processes simultaneously.

1.3 Carbon Fiber Microelectrodes

Carbon fibers exhibit truly outstanding properties. Their strength, competes with the strongest steels; they can have stiffness, E, greater than any metal, ceramic or polymer; and they can exhibit thermal and electrical conductivities that greatly exceed those of competing materials. If the strength or stiffness values are divided by the low density, 1800-2100 kg m^{-3}, then their huge specific properties make this class of materials quite unique.

Polyacrylonitrile (PAN) type carbon fiber, produced by carbonization of PAN precursor, having high tensile strength and high elastic modulus, extensively applied for structural material composites in aerospace and industrial field and sporting recreational goods.

PAN based fibers are produced from a solubilized mixture that is wet or dry spun to produce a fiber, ostensibly for use in the textile industry. This fiber is stabilized and carbonized to produce a carbon fiber. Aerospace grade material can be obtained in tows that contain between 3000 and 12000 fibers. Lower performance materials are usually formed using larger tows that contain up to 320000 fibers. PAN based carbon fibers are cheaper when produced from larger tows.

Pitch type of the fiber, produced by carbonization of oil/coal pitch precursor, having extensive properties from low elastic modulus to ultra high elastic modulus.

Fibers with ultra high elastic modulus are extensively adopted in high stiffness components and various uses as utilizing high thermal conductivity and / or electric conductivity. Pitch fibers are melt spun products obtained in small tow sizes varying from 2000 to 4000 fibers. They are usually larger diameter (10-15 pm) than fibers formed from PAN.

The most important mechanical and physical properties exhibited by carbon fibers are the elastic modulus, tensile strength, electrical and thermal conductivities. Carbon fibers are used in fiber-reinforced composites, which consist of fiber and resin. Original large-scale applications were in the reinforcement of polymers. As the technology of textile reinforced composites expanded, a growing demand from the aerospace industry for composite materials with superior properties emerged. In particular, materials with higher specific strength, higher specific modulus and low density were required.

Other desirable properties were good fatigue resistance and dimensional stability. Although carbon fibers meet these demands, it is necessary to improve interfacial properties between reinforcing (carbon) fibers and the polymeric matrix. The electrochemical deposition of conducting polymers on carbon substrates has been studied with the goal of improving the mechanical properties of conducting polymers, so as to use them as electrodes in different applications: electrochromic displays, batteries, sensors, capacitors.

Electropolymerization onto carbon fiber microelectrodes was performed by Sarac et al. Surface characterizations of thin film coating of random poly(N-vinylcarbazole-co-vinylbenzenesulfonic acid), [47,48] copolymer on carbon fiber was performed. Copolymer films of pyrrole and 3,4-ethylenedioxythiophene (EDOT) were synthesized electrochemically on the carbon fiber microelectrodes (CFME). Deposition conditions on the carbon fiber and influence of the monomer concentrations to the copolymerization as well as the electrochemistry of the resulting polymers and copolymers were studied using cyclic voltammetry, in-situ spectroelectrochemistry, FTIR-ATR and scanning electron microscopy [49].

Thin film electro-coated poly(N-vinylcarbazole-co-vinylbenzene sulfonic acid) [50,51] p(NVCzVBSA), poly(carbazole-co-methylthiophene), (p(CzMeTh) and polycarbazole (p(Cz)) coated carbon fibre microelectrodes (CFMEs) were characterized by scanning electron microscopy (SEM) and FTIR-ATR spectroscopy.

1.4 Electrochemical Impedance Spectroscopy (EIS)

Electrical resistance is the ability of a circuit element to resist the flow of electrical current. Ohm's law (Equation 1.6) defines resistance in terms of the ratio between voltage E and current I.

$$R = \frac{E}{I} \tag{1.6}$$

While this is a well known relationship, it's use is limited to only one circuit element the ideal resistor. An ideal resistor has several simplifying properties:

· It follows Ohm's Law at all current and voltage levels.

· It's resistance value is independent of frequency.

· AC current and voltage signals though a resistor are in phase with each other.

The real world contains circuit elements that exhibit much more complex behavior. These elements force us to abandon the simple concept of resistance. In its place impedance is used, which is a more general circuit parameter.

Impedance is a totally complex resistance encountered when a current flows through a circuit made of resistors, capacitors, or inductors, or any combination of these. Depending on how the electronic components are configured, both the magnitude and the phase shift of an ac can be determined.

Because an inductive effect is not usually encountered in electrochemistry, it is considered that only the simple equivalent circuit shown in Figure 1.12 in which no inductor is present.

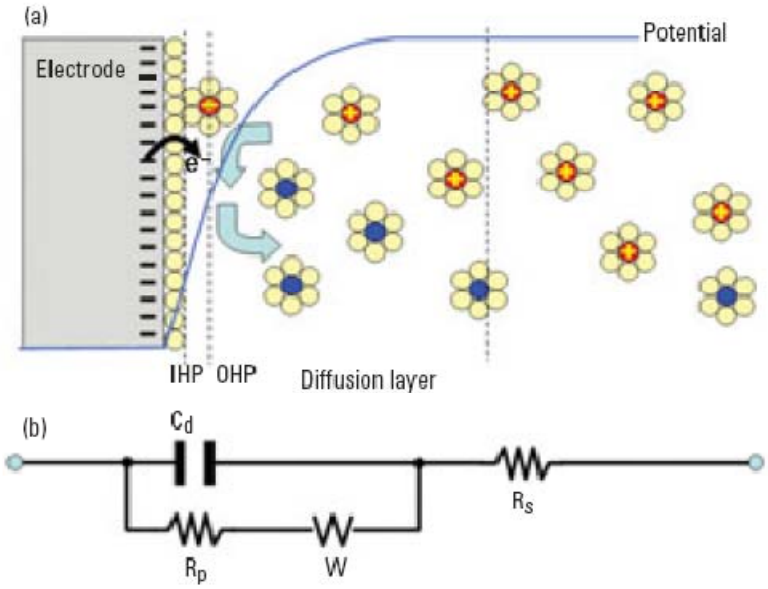

Figure 1.11 (a) The oxidants (red) with a positive charge diffuse toward the negatively charged electrode, acceptelectrons from the electrode at the interface, become the reductants (blue), and diffuse to the bulkof the solution. The oxidant is also a counterion to the electrode. No specific adsorption is consideredat the interface. IHP and OHP are the inner and outer Helmholtz planes, respectively. (b) An equivalent circuit representing each component at the interface and in the solution during an electrochemicalreaction is shown for comparison with the physical components. C_{dl}, double layer capacitor; Rp, polarization resistor; W, Warburg resistor; R_s, solution resistor.

However, first consider an experiment in which a series of increasing dc potentials (a ramp) are applied to a working electrode in an electrochemical cell containing an electroactive species.

$$i = i_0 \left[e^{\frac{-\alpha n F}{RT}\eta} - e^{\frac{(1-\alpha) n F}{RT}\eta} \right] \qquad \textbf{(1.7)}$$

A current – potential curve (Figure 1.12) is obtained, which is described by the Butler–Volmer equation (solid line) in which η is the overpotential defined as $E - E_{eq}$, with E and E_{eq} representing the applied and equilibrium potentials, respectively; i_o is the exchange current at η= 0; n is the number of electrons transferred; F is the Faraday constant; R is the gas constant; T is the absolute temperature; and α is the transfer coefficient for electron transfer. The faradaic current i is limited by the mass transport (dashed line curving to the right) when the rate of electron transfer becomes large enough. At a given overpotential η_{bias}, the slope of the curves, $di/d\eta_{bias}$, is $1/R_P$, in which R_p is the polarization resistance.

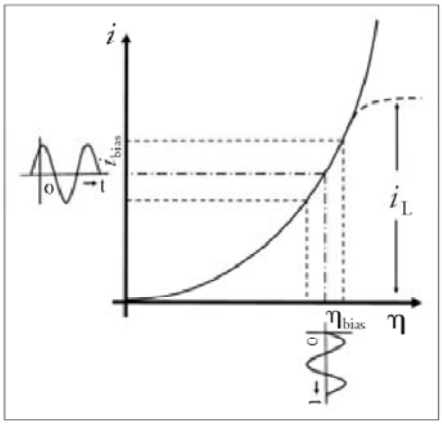

Figure 1.12 The DC plotted as a function of overpotential according to the Butler-Volmer equation (solid line), which is limited by mass transport at large overpotentials (dashed line curving to the right), an ac voltage (broken line) superimposed on the dc bias potential, _bias (dot-dashed line), shown on the *i* axis [ηbias + ηsin(ωt)], and the resulting ac superimposed on the dc on the *i* axis [*i*bias + _*i*sin(ωt +Ø)]. *R*p is obtained by taking _η/_*i*, in which *i* is obtained after applying the ac voltage wave at a given η.

When a small ac voltage wave of frequency ω at η bias is superimposed, the ac of the same frequency will be flowing on top of the dc. Because the interface has resistors and a capacitor (Figure 1b), the flowing ac will experience a phase shift, expressed as i_{bias}, caused by the ac wave perturbation. For an equivalent circuit, a straightforward impedance expression can be derived by applying Ohm's law to two components connected in parallel. One of these is R_p, and the other is 1/(jωCd), in which C_{dl} (or C_d) is the double-layer capacitance.

$$Z(\omega) = R_s + \frac{R_p}{1 + j\omega R_p C_d} =$$

$$R_s + \frac{R_p}{1 + \omega^2 R_p^2 C_d^2} - \frac{j\omega R_p^2 C_d}{1 + \omega^2 R_p^2 C_d^2} = Z' + jZ'' \qquad \textbf{(1.8)}$$

To make the derivation of the equation and its interpretation straightforward, the contribution of the Warburg component is neglected. Thus, the impedance of the interface consists of two parts, a real number Z' and an imaginary number Z'' with a complex representation, $Z(\omega) = Z'(\omega) + jZ''(\omega)$ with Ø (the phase angle) = $\tan^{-1}[Z''(\omega)/Z'(\omega)]$. Although the capacitance is relatively constant over the potential at a given electrode, the R_p varies as a function of ηbias applied to the electrode. At a given dc bias potential, a series of $Z(\omega)$ data are obtained in a range of frequencies, typically 100 kHz^{-1} to 10^{-4} Hz. The impedance varies, depending on frequencies, and is often plotted in different ways as a function of frequency (making it a spectroscopic technique), hence, the name EIS [52-57].

By treating the impedance data in such a frequency range, system characteristics for an electrochemical reaction (i.e., *R*s, *R*p, and C_{dl}) can be obtained. R_p is a function of potential; however, at $\eta = 0$, it becomes the charge-transfer resistance R_{CT}. Two convenient ways of treating the impedance data are the Nyquist plot, (Figure1.11a) in which imaginary numbers $Z''(\omega)$ are plotted against real numbers $Z'(\omega)$, and the Bode plot, (Figure 1.11b) in which absolute values of impedance or phase angle are plotted against the frequency. Extraction of the system characteristics requires interpreting the Nyquist plot according to Equation (1.8).

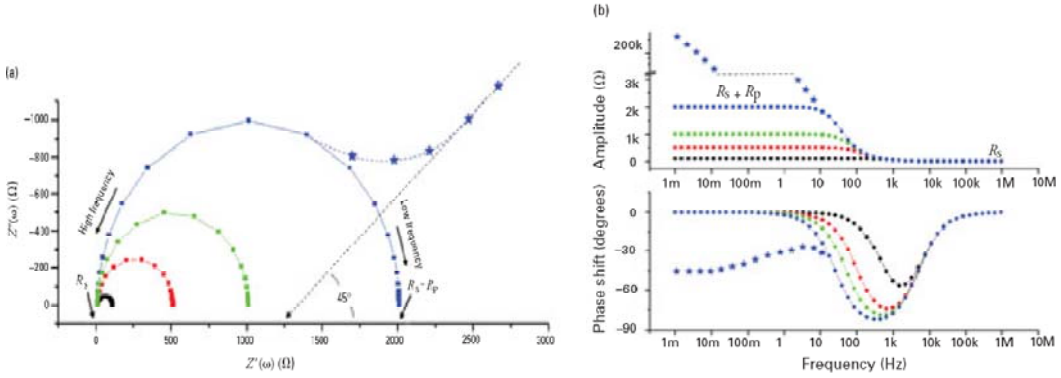

Figure 1.13: (a) Nyquist plot **(b)** Bode magnitude of Z and Bode phase angle

At high frequencies, the frequency dependent term of Equation 1.8 vanishes, resulting in $Z(\omega) = Z'(\omega) = R_s$, which is an intercept on the $Z'(\omega)$ axis on the high frequency side ($\emptyset = 0$ or $Z''(\omega) = 0$). For $\omega \rightarrow 0$, Equation 1.8 becomes $Z(\omega) = R\text{s} + R\text{p}$, which is an intercept on the $Z'(\omega)$ axis on the lowfrequency side. At the frequency where a maximum $Z''(\omega)$ is observed, the straightforward relationship $R_p.C_d = 1/\omega_{max} = 1/(2\pi f_{max}) = \zeta_{rxn}$, which is the time constant of the electrochemical reaction, can be shown and indicates how fast the reaction takes place.

Also, if $R_p.C_d$ is known, C_d can be obtained because R_p is already known from the low-frequency intercept on the $Z'(\omega)$ axis. The Nyquist plot gives all the necessary information about the electrode–electrolyte interface and the reaction. Similar information is obtained by examining the Bode diagram using Equation 1.8. Log R_s and log (R_p+R_s) are obtained straight forwardly from the $Z(\omega)$ versus logω plot at high and low frequencies from the same argument as the Nyquist plot. The equation for this line is obtained by ignoring the frequency-independent terms, R_s and 1 in the denominator, of Equation 1.8 to yield :

$$Z(\omega) - R_s + \frac{R_p}{1 + j\omega R_p C_d} \quad \textbf{(1.9)}$$

Taking the logarithm on both sides of the resulting equation yields log $Z(\omega) = -\log \omega - \log C_d$, which indicates that log $|Z(\omega)|$ versus log ω would have a slope of –1, and C_{dl} can be obtained from the intercept of this line with the $Z(\omega)$ axis when $-\log \omega = 0$ at $\omega = 1$. Thus, the Bode plot provides the same information as the Nyquist plot. The Ø versus log ω plot shows that the impedance responses are resistive primarily at high and low frequencies as indicated by practically no phase shifts, whereas at intermediate frequencies, they are mostly capacitive as their phase shifts get closer to 90^o.

The equivalent circuit without considering the effect of the Warburg impedance can be discussed; however, its contribution can be important at low frequencies because the mass transport of the electroactive species may limit the electron transfer process. The Warburg impedance [58] is imparted by mass transfer.

Measuring impedance principle is the basis on which impedance is measured: A small ac wave, typically 5–10 mV (peak-to-peak) of a given frequency, is superimposed on the dc η_{bias}, and the resulting ac and its phase shift i_{bias} are measured.

These measurements may be made in various ways [59-61]; however, the frequency response analyzer has become the industry standard in electrochemical instrumentation in recent years. The reference ac wave of frequency super imposed on a given dc bias potential is applied to a working electrode in the electrochemical cell. The ac signal S(t) obtained from the cell is then multiplied by the reference sine or cosine wave and integrated to obtain.

1.4.1 Equivalent Circuit Elements

Solution resistance is often a significant factor in the impedance of an electrochemical cell. A modern 3 electrode potentiostat compensates for the solution resistance between the counter and reference electrodes. However, any solution resistance between the reference electrode and the working electrode must be considered when the cell is simulated.

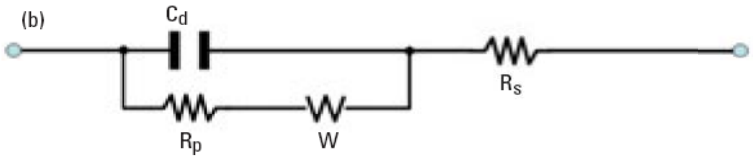

Figure 1.14: An equivalent circuit representing each component at the interface and in the solution during an electrochemical reaction is shown for comparison with the physical components. C_{dl}, double layer capacitor; R_p, polarization resistor; W, Warburg resistor ; R_s, solution resistor.

The resistance of an ionic solution depends on the ionic concentration, type of ions, temperature and the geometry of the area in which current is carried. In a bounded area with area A and length l carrying a uniform current the resistance is defined as:

$$R = \rho \frac{l}{A} \tag{1.10}$$

where r is the solution resistivity.

The conductivity of the solution, k , is more commonly used in solution resistance calculations. Its relationship with solution resistance is:

$$R = \frac{1}{\kappa} \frac{l}{A} \Rightarrow \kappa = \frac{l}{RA} \tag{1.11}$$

Standard chemical handbooks list k values for specific solutions. For other solutions, k can be calculated from specific ion conductances. The units for k are siemens per meter (S/m). The siemens is the reciprocal of the ohm, so 1 S = 1/ohm. The value of the double layer capacitance depends on many variables including electrode potential, temperature, ionic concentrations, types of ions, oxide layers, electrode roughness, impurity adsorption, etc.

A electrical double layer exists at the interface between an electrode and its surrounding electrolyte.

This double layer is formed as ions from the solution "stick on" the electrode surface. Charges in the electrode are separated from the charges of these ions. The separation is very small, on the order of angstroms.

Whenever the potential of an electrode is forced away from it' s value at open circuit, that is referred to as polarizing the electrode. When an electrode is polarized, it can cause current to flow via electrochemical reactions that occur at the electrode surface.

The amount of current is controlled by the kinetics of the reactions and the diffusion of reactants both towards and away from the electrode.

In cells where an electrode undergoes uniform corrosion at open circuit, the open circuit potential is controlled by the equilibrium between two different electrochemical reactions. One of the reactions generates cathodic current and the other anodic current. The open circuit potential ends up at the potential where the cathodic and anodic currents are equal. It is referred to as a mixed potential. The value of the current for either of the reactions is known as the corrosion current. A new parameter, R_p, the polarization resistance.

Diffusion can create an impedance known as the Warburg impedance. This impedance depends on the frequency of the potential perturbation. At high frequencies the Warburg impedance is small since diffusing reactants don't have to move very far. At low frequencies the reactants have to diffuse farther, thereby increasing the Warburg impedance.

The equation for the "infinite" Warburg impedance is:

$$Z = \sigma(\omega)^{-1/2} (1-j) \qquad \textbf{(1.12)}$$

On a Nyquist plot the infinite Warburg impedance appears as a diagonal line with a slope of 0.5. On a Bode plot, the Warburg impedance exhibits a phase shift of 45°. Capacitors in EIS experiments often do not behave ideally. Instead, they act like a constant phase element (CPE) as defined below.

The impedance of a capacitor has the form:

$$Z = A(j\omega)^{-\alpha} \qquad \textbf{(1.13)}$$

When this equation describes a capacitor, the constant A = 1/C (the inverse of the capacitance) and the exponent a = 1. For a constant phase element, the exponent is less than one.

The "double layer capacitor" on real cells often behaves like a CPE instead of like like a capacitor. Several theories have been proposed to account for the non-ideal behavior of the double layer but none has been universally accepted [62].

1.5 Characterizations

1.5.1 Attenuated Total Reflection Fourier Transform Infrared Spectroscopy

Infrared spectroscopy is widely used in both research and industry as a simple and reliable technique for measurement, quality control, and dynamic measurement.

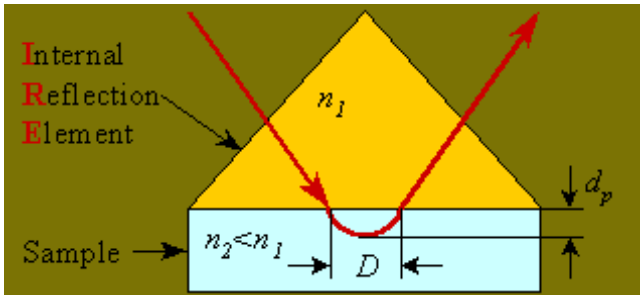

Figure 1.15: Schematic representation of path of a ray of light for total internal reflection (Single reflection). The ray penetrates a fraction of a wavelength (d_p) beyond the reflecting surface into the rarer medium of refractive index n_2 and there is a certain displacement (D) upon reflection, n_1 is refractive index of the interval reflection elements.

The instruments are now small, and can be transported, even for use in field trials. Attenuated total reflectance (ATR) spectroscopy, also known as internal reflection spectroscopy or multiple internal reflectances (MIR), is a versatile, nondestructive technique for obtaining the infrared spectrum of the surface of a material or the spectrum of materials either too thick or too strongly absorbing to be analyzed by standard transmission spectroscopy.

Attenuated Total Reflectance (ATR) spectroscopy, known as internal reflection spectroscopy or multiple internal reflectance (MIR), is a versatile, nondestructive technique for obtaining the infrared spectrum of the surface of material or the spectrum of materials either too thick or too strongly absorbing to be analyzed by standart transmission spectroscopy.

In this technique, the sample is placed in contact with the internal reflection element (IRE), the light is totally reflected, generally several times, and the sample interacts with the evanescent wave resulting in the absorption of radiation by the sample at each point of reflection.

The internal reflection element is made from a material with a high refractive index; zinc selenide (ZnSe), thallium iodide – thallium bromide (KRS-5), and germanium (Ge) are the most commonly used.

By measuring at a specific frequency over time, changes in the character or quantity of a particular bond can be measured. This is especially useful in measuring the degree of polymerization in polymer manufacture. Modern research machines can take infrared measurements across the whole range of interest as frequently as 32 times a second. This can be done whilst simultaneous measurements are made using other techniques. This makes the observations of chemical reactions and processes quicker and more accurate.

1.5.2 Atomic Force Microscopy (AFM)

For qualitative analysis in fractography, SEM (scanning electron microscopy) and stereoscopic techniques are widely used but are limited by quantitative measurements on the surface such as, roughness and striations on fractured surface. Therefore, the implementation of a reliable and specialized qualitative and quantitative technique that can reveal the three-dimensional characteristics of the surface and the study of related parameters is necessary.

At the microscopic and submicroscopic scales such possibility is now offered by atomic force microscopy (AFM).

Figure 1.16 [63] shows the AFM scheme, which consists of a cantilever and an integrated tip as shown in Figure 1.17 [64]. While the tip makes contact with the sample surface, a laser beam, focused on the back of the cantilever, reflects onto a quadrant photodetector. The deflection in cantilever due to applied normal and lateral forces can be measured by monitoring the variation in the photodetector signal. This allows the force detection in the nano-Newton to pico-Newton (10^{-9} to 10^{-12} N) regime.

The principles of operation of an AFM are very simple: an extremely, usually atomically, sharp tip made of Si or Si_3N_4 is micro machined at the end of a flexible cantilever. The sensors used in this study were of silicon. It is then positioned in close proximity of the sample surface, where the cantilever is bent by the atomic force between the tip and sample surface .The tip geometry that was used during this work is shown in Figure 1.17.

This tip is a contact mode nano-sensor, with a tip radius of 7 – 10 nm and 30 nm aluminum reflex coating on cantilever side that improves reflectivity.

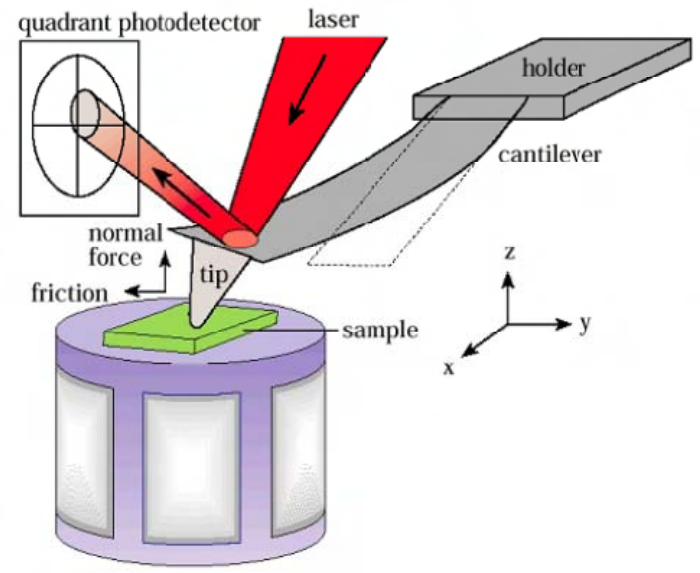

Figure 1.16: Squematic diagram of atomic force microscope

Figure 1.17: Squematic AFM contact mode probe

Magnification of the vertical surface features of an object, those features leaving the horizontal plane and extending in the vertical direction, have historically been measured by a stylus profiler. This profiler, invented by Schmalz in 1929, utilized an optical lever arm to monitor the motion of a sharp probe mounted at the end of a cantilever. A magnified profile of the surface was generated by recording the motion of the stylus on photographic paper.

This type of "microscope" generated profile "images" with a magnification of greater than 1000X. A common problem with stylus profilers was the possible bending of the probe from collisions with surface features. Such "probe bending" was a result of horizontal forces on the probe caused when the probe encountered large features on the surface.

This problem was first addressed by Becker in 1950 and later by Lee. Both Becker and Lee suggested oscillating the probe from a null position above the surface to contact with the surface. Becker remarked that when using this vibrating profile method for measuring images, the detail of the images would depend on the sharpness of the probe.

In 1971 Russell Young demonstrated a non-contact type of stylus profiler. In his profiler, called the topographiner, Young used the fact that the electron field emission current between a sharp metal probe and a surface is very dependent on the probe sample distance for electrically conductive samples. In the topographiner , the probe was mounted directly on a piezoelectric ceramic used to move the probe in a vertical direction above the surface. An electronic feedback circuit monitoring the electron emission was then used to drive the piezoceramic and thus keep the probe sample spacing fixed.

Then, with piezoelectric ceramics, the probe was used to scan the surface in the horizontal (XY) dimensions. By monitoring the X-Y and Z position of the probe, a 3-D image of the surface was constructed. The resolution of Young's instrument was controlled by the instrument's vibrations.

In 1981 researchers at IBM were able to utilize the methods first demonstrated by Young to create the scanning tunneling microscope (STM). Binnig and Rohrer demonstrated that by controlling the vibrations of an instrument very similar to Young's topographiner, it was possible to monitor the electron tunneling current between a sharp probe and a sample. Since electron tunneling is much more sensitive than field emissions, the probe could be used to scan very close to the surface. The results were astounding; Binnig and Rohrer [65] were able to see individual silicon atoms on a surface. Although the STM was considered a fundamental advancement for scientific research, it had limited applications, because it worked only on electrically conductive samples.

A major advancement in profilers occurred in 1986 when Binnig and Quate demonstrated the Atomic Force Microscope. Using an ultra-small probe tip at the end of a cantilever, the atomic force microscope could achieve extremely high resolutions. Initially, the motion of the cantilever was monitored with an STM tip. However, it was soon realized that a light-lever, similar to the technique first used by Schmalz, could be used for measuring the motion of the cantilever. In their paper, Binnig and Quate proposed that the AFM could be improved by vibrating the cantilever above the surface.

The first practical demonstration of the vibrating cantilever technique in an atomic force microscope was made by Wickramsinghe in 1987 with an optical interferometer to measure the amplitude of a cantilever's vibration.

Using this optical technique, oscillation amplitudes of between 3 nm and 100 nm were achieved. Because the probe comes into close contact with the surface upon each oscillation, Wickramsinghe was able to sense the materials on a surface. The differences between photo-resist and silicon were readily observed.

The AFM can be compared to traditional microscopes such as the optical or scanning electron microscopes for measuring dimensions in the horizontal axis.

However, it can also be compared to profilers for making measurements in the vertical axis to a surface. One of the great advantages of the AFM is the ability to magnify in the X, Y and Z axes.

When compared to a profiler, the AFM has a greater X-Y resolution because in the AFM the probe is sharper. Profilers can have high vertical resolutions, as low as 0.5 nm. However, the bandwidth of the profiler measurements is much lower than an AFM. To achieve a resolution of 0.5 nm a profile has a bandwidth of approximately 0.1 Hz. The AFM bandwidth for the equivalent measurement is between 5 kHz and 10Khz. The length scale of an optical microscope overlaps nicely with an AFM. Thus, an AFM is typically combined with an optical microscope and with this combination it is possible to have a field of view dynamic range from mm to nm. In practice, an optical microscope is typically used for selecting the location for AFM scanning.

The AFM is most often compared with the electron beam techniques such as the SEM or TEM. In general, it is easier to learn to use an AFM than an SEM because there is minimal sample preparation required with an AFM. With an AFM, if the probe is good, a good image is measured. A comparison of the some of the major factors follows as shown in Figure 1.18.

	SEM / TEM	AFM
Samples	Must be conductive	Insulating / Conductive
Magnification	2 Dimensional	3 Dimensional
Environment	Vacuum	Vacuum / Air / Liquid
Time for image	0.1 - 1 minute	1 - 5 minute
Horizontal Resolution	0.2 nm (TEM) 5 nm (FE-SEM)	0.2 nm
Vertical Resolution	n/a	.05 nm
Field of View	100 nm (TEM) 1 mm (SEM)	100 μm
Depth of Field	Good	Poor
Contrast on Flat Samples	Poor	Good

Figure 1.18: Comparison of an AFM and SEM.

SEM/TEM instruments are capable of doing much more than topography measurements. For example, electron beam instrumentation can do EDX measurements or even electron beam initiated lithography. Likewise, the AFM can make many types of measurements other than AFM topographical measurements. For example, AFM instruments can make thermal, magnetic and electric field maps of a surface. Like the SEM/TEM, an AFM can also initiate lithographic changes on a surface.

Although the time required for making a measurement with the SEM image is typically less than an AFM, the amount of time required to get meaningful images is similar. This is because the SEM/TEM often requires substantial time to prepare a sample. With the AFM, little or no sample preparation is required.

In comparison with an optical microscope and the SEM/TEM an AFM is more difficult to use than the optical microscope and easier to use than the SEM/TEM. Also, the AFM is typically more expensive than the optical microscope and less costly than an SEM/TEM. Figure 1.19 compares the relative time and cost for optical, AFM, and SEM/TEM microscopes.

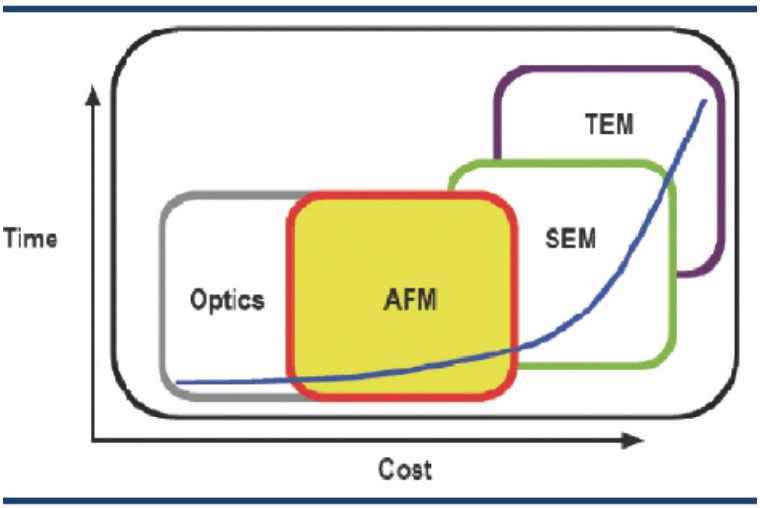

Figure 1.19: Comparison of the time for measurements and instrumentation cost optical, AFM, and SEM/TEM microscopes.

Lastly, an optical microscope requires the least amount of laboratory space, while the SEM/TEM requires the most amount of laboratory space. An AFM is in the middle of these two.

Finally, in comparison to an optical profiler, the AFM is more difficult to use. This is because the optical profiler does not need any adjustments. However, the AFM requires adjustments of the scan speed and the feedback control parameters [66].

1.5.3 Scanning Electron Microscope (SEM)

The scanning electron microscope (SEM) is a type of electron microscope capable of producing high resolution images of a sample surface. SEM images have a characteristic three-dimensional appearance and are useful for judging the surface structure of the sample.

In a typical SEM electrons are thermionically emitted from a tungsten or lanthanum hexaboride (LaB_6) cathode and are accelerated towards an anode; alternatively electrons can be emitted via field emission (FE). Tungsten is used because it has the highest melting point and lowest vapour pressure of all metals, thereby allowing it to be heated for electron emission. The electron beam, which typically has an energy ranging from a few hundred eV to 50 keV, is focused by one or two condenser lenses into a beam with a very fine focal spot sized 1 nm to 5 nm.

The beam passes through pairs of scanning coils in the objective lens, which deflect the beam in a raster fashion over a rectangular area of the sample surface.

Through these scattering events, the primary electron beam effectively spreads and fills a teardrop-shaped volume, known as the interaction volume, extending from less than 100 nm to around 5 μm into the surface. Interactions in this region lead to the subsequent emission of electrons which are then detected to produce an image. X-rays, which are also produced by the interaction of electrons with the sample, may also be detected in an SEM equipped for energy-dispersive X-ray spectroscopy or wavelength dispersive X-ray spectroscopy.

The nature of the SEM's probe, energetic electrons, makes it uniquely suited to examining the optical and electronic properties of semiconductor materials. The high-energy electrons from the SEM beam will inject charge carriers into the semiconductor. Thus, beam electrons lose energy by promoting electrons from the valence band into the conduction band, leaving behind holes [67].

2. EXPERIMENTAL

2.1 Chemicals

Sodium perchlorate ($NaClO_4$) from Fluka and acetonitrile (ACN) from Riedel de Haen were used without further purification. The ProDOT-Bu_2 monomer was synthesized in three steps from commercially available starting materials using Mitsunobu conditions [68] followed by alkaline hydrolysis [69] and decarboxylation [70] of the resulting precursor.

2.2 Preparation of Single Carbon Fiber Microelectrodes

Carbon fibers were prepared in our laboratory by a specific method. At first, a single carbon fiber SGL SIGRAFIL HM48 (7µm in diameter, approx. 4 cm in length) was inserted onto 5 cm length sticky tape while 1.5 cm of fiber was kept out of . After that, a filament of carbon fibers with a length of 8 cm (approximately 25 fibers) were sticked with placing onto the single carbon fiber for electrical conduction of single fiber, second sticky tape with the same length was placed and electrical conductivity was tested with a multimeter. Then SCFME was initially cleaned in acetone for 2 minutes, then rinsed with distelled water and dried at room temprature.

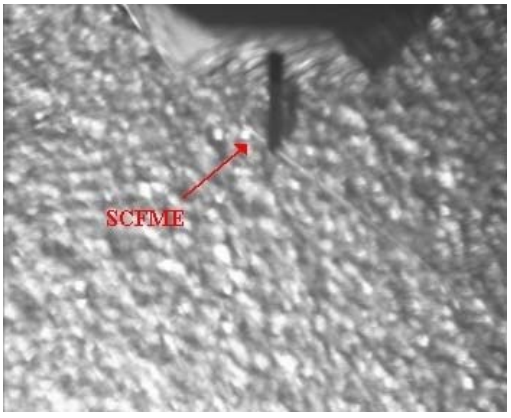

Figure 2.1: Top view image of a SCFME with an optical microscope

2.3 Electropolymerization, Cyclic Voltammetric Study

Electropolymerization was performed in 0.1M $NaClO_4$/ACN. A Parstat 2263 potentiostat (Princeton Applied Research), a self-contained unit that combines potentiostat circuitry with phase sensitive detection (Faraday cage that Bass Cell Stand C3), was used for cyclic voltammetry (CV). Electropolymerisation was performed using a three electrode system with a SCFME, Pt wire or ITO coated glass as a working electrode, a platinum (Pt) wire as a counter and a silver (Ag) wire as a pseudoreference electrode; the cell has a volume of 5 mL solution, arrange in a way at a distance of, 1 cm from each other. The pseudoreference electrode was calibrated externally using a 5 mM solution of ferrocene/ferrocenium (Fc/Fc^+) couple in the electrolyte and potentials were reported vs. the Ag electrode.

2.4 Characterization

Electrochemical impedance measurements were conducted in monomer free electrolyte solution with a 10 mV perturbation amplitude between a frequency range of 0.01Hz-100 kHz with PARSTAT 2263-1 with using powersuite software. The electrochemical parameters of the p(ProDOT-Bu_2) were evaluated by employing the ZSimpWin (version 3.10) software from Princeton Applied Research. R(C(R(Q(RW))))(CR) equivalent circuit model was studied with resulted impedance data.

The substrate surfaces coated with polymer by electrochemical polymerisation were analysed using an ATR-FTIR reflectance spectrophotometer (PerkinElmer, Spectrum One; with a universal ATR attachment with a diamond and ZnSe crystal C70951).

The AFM images reported in this study were obtained with Nanosurf Easy Scan 2 ™ AFM. In all AFM analysis, the non-contact mode was employed by using Al coated high resonance frequency silicon tips (190 kHz) with 7μm thickness, 38μm mean width, 225μm length and 48N/m force constant. High resolution images and the raw data collected by the Easy Scan 2 Software™ (version 1.5.0.0.) using left shadowing.Morphology of conducting polymer nanotubules was investigated via a high resolution Supra Gemini 35VP Field Emission Scanning Electron Microscope from LeoImaging was generally operated at 2 keV accelerating voltage, using the secondary electron imaging technique.

3. RESULTS AND DISCUSSION

3.1 Electropolymerizations of ProDOT-Bu_2 on CFMEs

Poly(2,2-Dibuthyl-3,4-propylenedioxythiophene) (PProDOT-Bu_2) thin films have been cyclovoltametrically coated onto micron size single carbon fiber microelectrodes (SCFME). An electrochemical impedance spectroscopic study (EIS) on the prepared electrodes is reported in this part which electropolymerization performed with different cycles (1, 3, 5, 10, 15 and 20) in the 0,1 M $NaClO_4$ / ACN solution. The electrochemical impedance data fitted to equivalent circuit model, used to find out quantitative relationships between the suggested circuit components. Effect of the cycle number (total charge) on the capacitive behavior of the P(ProDOT-Bu_2) SCFME's and morphology of films obtained by AFM and SEM were discussed.

3.1.1 Electropolymerization and characterization of PProDOT-Bu_2 on SCFMEs

Schematic polymerization of ProDOT-$(Bu)_2$ on SCFME are illustrated in figure 3.1. The radical cation structures are formed in electrolyte with applying potential follows coupling reaction and results with ordered polymer chains due to close form of 3- and 4-positions of thiophene ring.

Electropolymerization processes were performed in 0.1 M $NaClO_4$/ACN with various cycles (1, 3, 5, 10,15 and 20 cycles). ACN was chosen as a standard solvent to prepare electrolyte for 0.01 M ProDOT-$(Bu)_2$ solution during this study. Electropolymerization of ProDOT-$(Bu)_2$ SCFMEs were achieved by cyclic voltammetry between 0-1.6 V at a scan rate of 100mVs^{-1} given in figures 3.2 -3.7.

The current increases with the cycle, indicates insoluble polymer film was coated on SCFME. Multisweep cyclic voltammogram of 10^{-2} M ProDOT$(Bu)_2$ also shows an increasing current density with each cycle and all anodic and corresponding cathodic peaks can be easily seen after 10^{th} cycle (E_{pa1} = 0.22V , E_{pa2} = 0.45V, E_{pa3} = 1.3V, E_{pc1}= 0.2V, E_{pc2}=0.35V, E_{pc3}=0,9V for Figure 3.5), resulting in the formation of thin films of conductive polymer on SCFME at 100 mVs^{-1} scan rate.

SCFMEs were washed throughly with ACN after electropolymerization and the scan rate dependence of all polymer films in monomer free solutions were investigated. Inset figures of Figure 3.2 to 3.7 shows redox behaviour of the polymer films on the SCFME in 0.1 M $NaClO_4$ monomer free solution with different scan rates. 3 redox couples which are obtained by CVs in monomer free solution are roughly corresponding to the electron transfer peaks. (First redox couple can be only seen clearly in Figure 3.4)

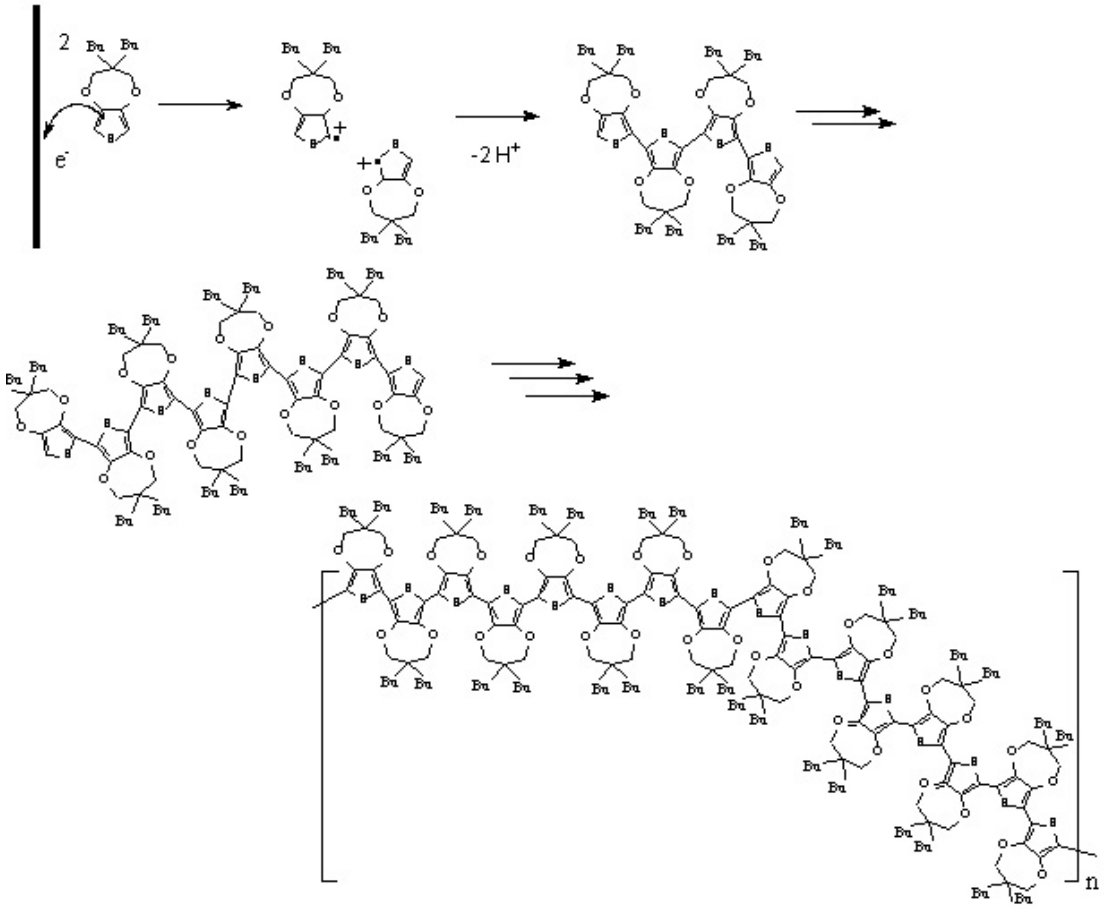

Figure 3.1: Electropolymerization of PProDOT-Bu_2 on SCFMEs

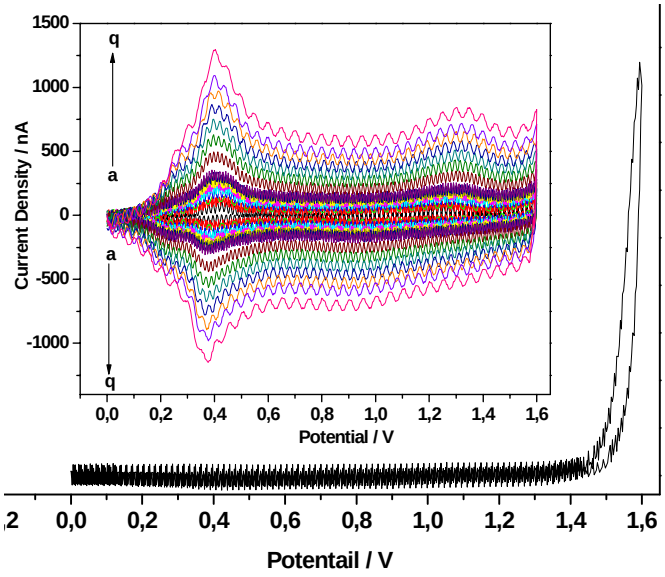

Figure 3.2 : Cyclic voltammetry of electrogrowth of 10^{-2} M ProDOT(Bu)$_2$ in 0.1 M $NaClO_4$/ACN; scan rate:100 mV/s; scan number: 1 cycle on CFME . Inset: P[ProDOT(Bu)$_2$] obtained under conditions described in cycled in different scan rates; a)50 mVs^{-1} , b)100 mVs^{-1} , c)150 mVs^{-1} , d) 200 mVs^{-1} , e)250 mVs^{-1} , f)300 mVs^{-1} , g) 350 mVs^{-1} , h)400 mVs^{-1} , i)450 mVs^{-1} , j)500 mVs^{-1} , k)750 mVs^{-1} l)1000 mVs^{-1} , m)1250 mVs^{-1} , n)1500 mVs^{-1} , o)2000 mVs^{-1} , p)2250 mVs^{-1} , q)2500 mVs^{-1} in 0.1 M $NaClO_4$/ACN. Q_{dep}:1.91µC

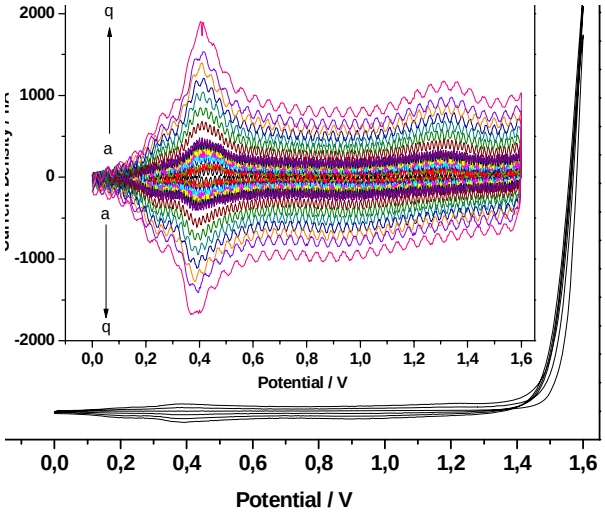

Figure 3.3 : Cyclic voltammetry of electrogrowth of 10^{-2} M ProDOT(Bu)$_2$ in 0.1 M $NaClO_4$/ACN; scan rate:100 mV/s; scan number: 3 cycles on CFME . Inset: P[ProDOT(Bu)$_2$] obtained under conditions described in cycled in different scan rates; a)50 mVs^{-1} , b)100 mVs^{-1} , c)150 mVs^{-1} , d) 200 mVs^{-1} , e)250 mVs^{-1} , f)300 mVs^{-1} g), 350 mVs^{-1} , h)400 mVs^{-1} , i)450 mVs^{-1} , j)500 mVs^{-1} , k)750 mVs^{-1} , l)1000 mVs^{-1} , m)1250 mVs^{-1} , n)1500 mVs^{-1} , o)2000 mVs^{-1} , p)2250 mVs^{-1} , q)2500 mVs^{-1} in 0.1 M $NaClO_4$/ACN. Q_{dep}: 10.5 µC

Up to 10 cycles, both anodic and cathodic peaks can not be visually detected during the electrogrowth of polymer thin films by CV, scan rate dependencies of these polymeric thin films at high scan rates shows good reversibility in first and second redox couples. But anodic peak potential of third redox couple shifts in the positive direction and cathodic peak potential of the redox couple shifs to negative potential.

The anodic and cathodic peak potentials of the films were independent on the scan rate, and the thin films could be cycled repeatedly between 50-2500 mVs^{-1} indicating the high stability of the polymer film without any decomposition below 10 cycles at very high scan rates.

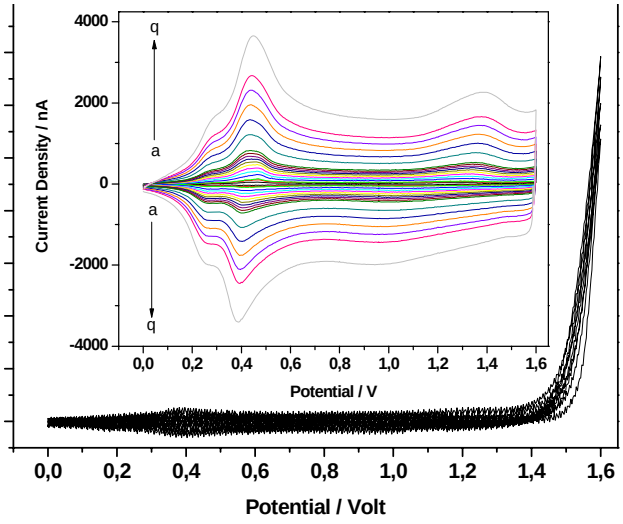

Figure 3.4 : Cyclic voltammetry of electrogrowth of 10^{-2} M ProDOT(Bu)$_2$ in 0.1 M $NaClO_4$/ACN; scan rate:100 mV/s; scan number: 5 cycles on CFME . Inset: P[PProDOT(Bu)$_2$] obtained under conditions described in cycled in different scan rates; a)50 mVs^{-1} , b)100 mVs^{-1} , c)150 mVs^{-1} , d) 200 mVs^{-1} , e)250 mVs^{-1} , f)300 mVs^{-1} , g) 350 mVs^{-1} , h)400 mVs^{-1} , i)450 mVs^{-1} , j)500 mVs^{-1} , k)750 mVs^{-1} , l)1000 mVs^{-1} , m)1250 mVs^{-1} , n)1500 mVs^{-1} , o)2000 mVs^{-1} , p)2250 mVs^{-1} , q)2500 mVs^{-1} in 0.1 M $NaClO_4$/ACN. Q_{dep} :33.2 µC

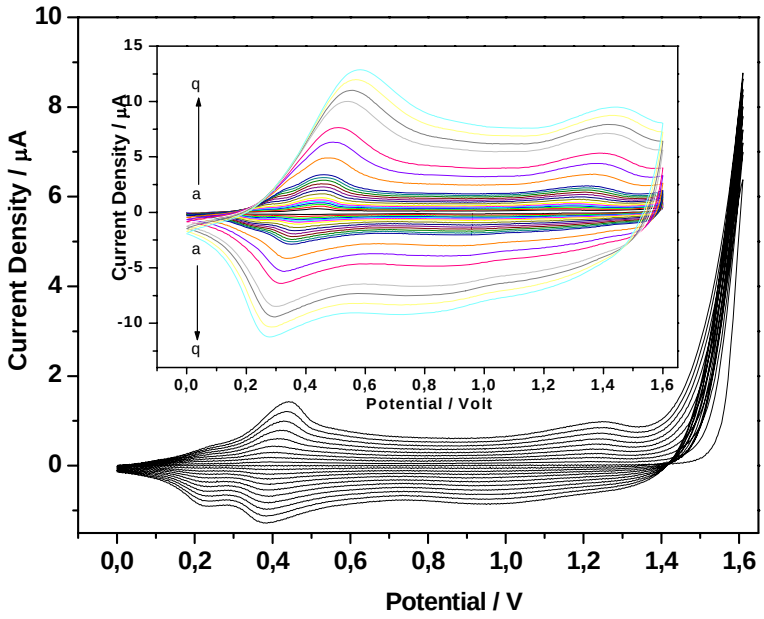

Figure 3.5 : Cyclic voltammetry of electrogrowth of 10^{-2} M ProDOT(Bu)$_2$ in 0.1 M $NaClO_4$/ACN; scan rate: 100 mV/s; scan number: 10 cycles on CFME . Inset: P[PProDOT(Bu)$_2$] obtained under conditions described in cycled in different scan rates; a)50 mVs^{-1} , b)100 mVs^{-1} , c)150 mVs^{-1} , d) 200 mVs^{-1} , e)250 mVs^{-1} , f)300 mVs^{-1} g), 350 mVs^{-1} , h)400 mVs^{-1} , i)450 mVs^{-1} , j)500 mVs^{-1} , k)750 mVs^{-1} , l)1000 mVs^{-1} , m)1250 mVs^{-1} , n)1500 mVs^{-1} , o)2000 mVs^{-1} , p)2250 mVs^{-1} , q)2500 mVs^{-1} in 0.1 M $NaClO_4$/ACN. Q_{dep}: 110.4 µC

Almost same anodic and cathodic peak potentials were obtained at varied scan rates for modified electrodes obtained up to 10 cycles which is a similar behaviour for the adsorbtion of species on the electrode surface where ΔE value almost so small. In contrast, the oxidation and reduction couple potentials shifted negatively and positively, after 10 cycles ΔE value ($\Delta E = E_a - E_p$) increases. During the scan rate dependency measurements in monomer free solution, this is a clear indication of changes of surface morphology of polymer thin film on the SCFME. However, (it will be discussed in later sections) uncoated regions of SCFMEs are started to disappear and a nano-villus like film was obtained at 20th cycle.Scan rate dependencies of the polymer films were investigated for the peak currents of 2nd and 3rd redox couples (1st redox couple is not shown due to overlapping with 2nd couple far all except 5 cycles) using current density values with respect to the scan rate instead of square root of scan rate which indicates a diffusion limited process of films.Correlation coefficient of the oxidation and reduction peaks for second and third redox couples were calculated as in the range of 0,999 – 0,986 indicate a thin-layer behaviour of the films [71].

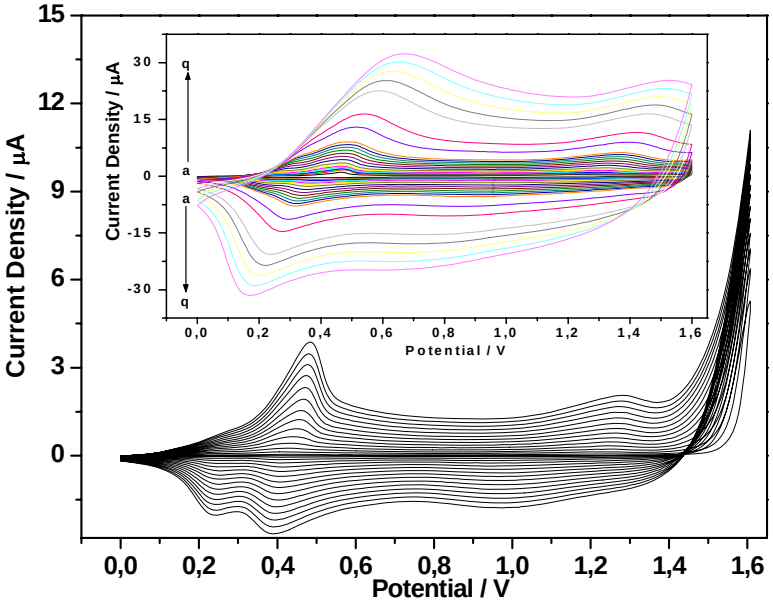

Figure 3.6 : Cyclic voltammetry of electrogrowth of 10^{-2} M ProDOT(Bu)$_2$ in 0.1 M $NaClO_4$/ACN; scan rate:100 mV/s; scan number: 15 cycles on CFME . Inset: P[PProDOT(Bu)$_2$] obtained under conditions described in cycled in different scan rates; a)50 mVs^{-1} , b)100 mVs^{-1} , c)150 mVs^{-1} , d) 200 mVs^{-1} , e)250 mVs^{-1} , f)300 mVs^{-1} , g) 350 mVs^{-1} , h)400 mVs^{-1} , i)450 mVs^{-1} , j)500 mVs^{-1} , k)750 mVs^{-1} , l)1000 mVs^{-1} , m)1250 mVs^{-1} , n)1500 mVs^{-1} , o)2000 mVs^{-1} , p)2250 mVs^{-1} , q)2500 mVs^{-1} in 0.1 M $NaClO_4$/ACN. Q_{dep}: 190.2 µC.

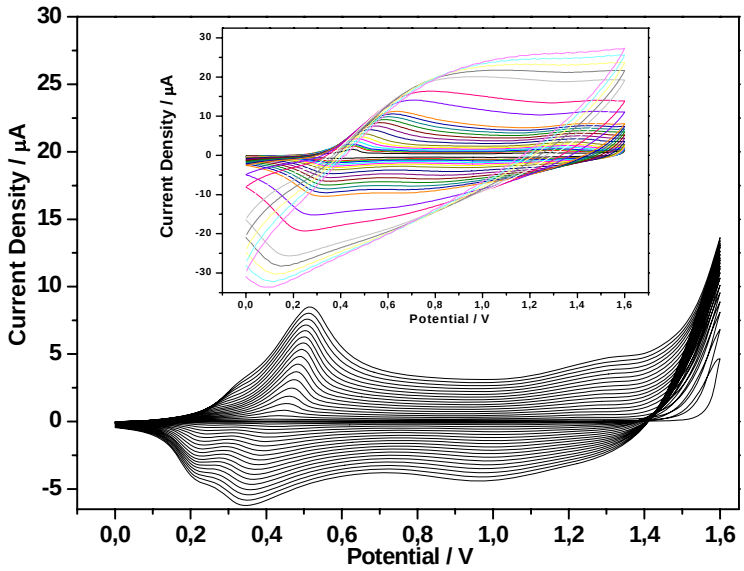

Figure 3.7 : Cyclic voltammetry of electrogrowth of 10^{-2} M ProDOT(Bu)$_2$ in 0.1 M $NaClO_4$/ACN; scan rate: 100 mV/s; scan number: 20 cycles on CFME . Inset: Poly[PProDOT(Bu)$_2$] obtained under conditions described in cycled in different scan rates; a)50 mVs^{-1} , b)100 mVs^{-1} , c)150 mVs^{-1} , d) 200 mVs^{-1} , e)250 mVs^{-1} , f)300 mVs^{-1} , g) 350 mVs^{-1} , h)400 mVs^{-1} , i)450 mVs^{-1} , j)500 mVs^{-1} , k)750 mVs^{-1} , l)1000 mVs^{-1} , m)1250 mVs^{-1} , n)1500 mVs^{-1} , o)2000 mVs^{-1} , p)2250 mVs^{-1} , q)2500 mVs^{-1} in 0.1 M $NaClO_4$/ACN. Q_{dep}: 417.5 µC.

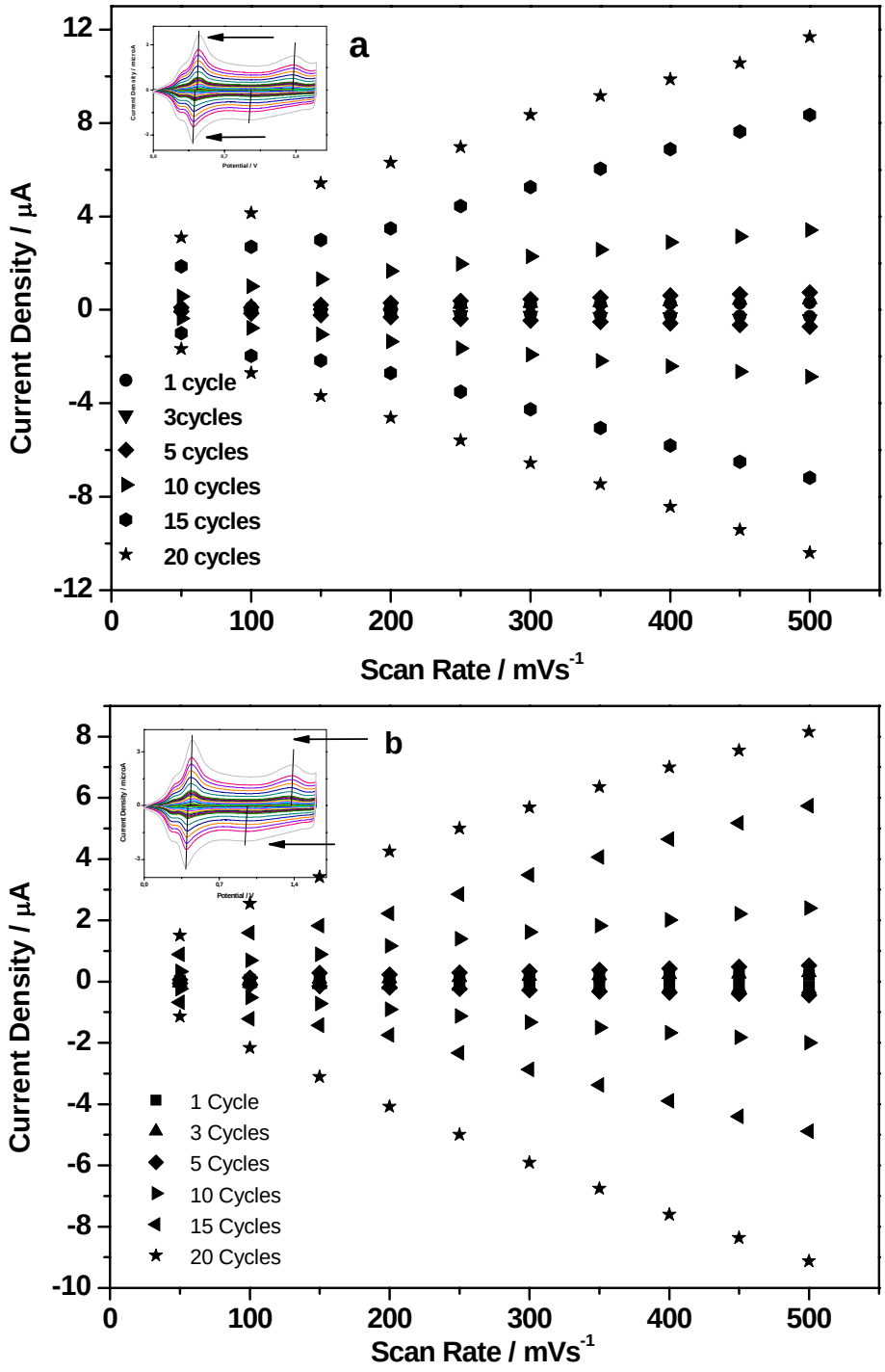

Figure 3.8 : a) Plot of second anodic and corresponding cathodic peak current density vs. the scan rate of the polymer film up to 500 mVs^{-1} in monomer free solution in 0.1 M $NaClO_4$/ ACN. b) Plot of third anodic and corresponding cathodic peak current density vs. scan rate dependence of the polymer film up to 500 mVs^{-1} in monomer free solution in 0.1 M $NaClO_4$/ ACN.

3.1.2 EIS and Equivalent Circuit Modelling of PProDOT-Bu_2 on SCFMEs

EIS measurements were performed at different cycles of the PProDOT-Bu_2 in monomer free electrolyte solution where stability of the film exhibit good electroactivity without undergoing deformation.

Figure 3.8 illustrates Nyquist plots of the PProDOT-Bu_2 film where the magnitude of the imaginery parts are very large for all cycles and system shows capacitive behaviour for all.

Figure 3.9 shows Bode magnitude and phase angle plots at which the frequency dependence of the system is more informative compared to Nyquist plots. The complex plane impedance plots demonstrate a vertical line with a phase angle very close to -85^o and bode phase plots also shows a shift to lower frequency while the bode magnitude curve of each cycles also show shift to lower frequency region with a constant slope of linear part indicating an increament of double layer capacitance (C_{DL}) with increasing the cycle numbers in bode magnitude plot (Table 1).

The low frequency capacitance (C_{LF}) values from impedance spectroscopy were obtained from the slope of a plot of the imaginary component (Z_{IM}) of the impedance at low frequencies versus inverse of the reciprocal frequency (f) where (f = 0.01 Hz) using following equation [72];

$$(C_{LF} = -1/2\pi f Z_{im}) \qquad \textbf{(3.1)}$$

The variation of the C_{LF} and the phase angle were showed with respect to the cycle number (Table 3.1.). The phase angle varies in a narrow range around -8^o while the C_{LF} increases significantly as the cycle number increases after 10 cycles.

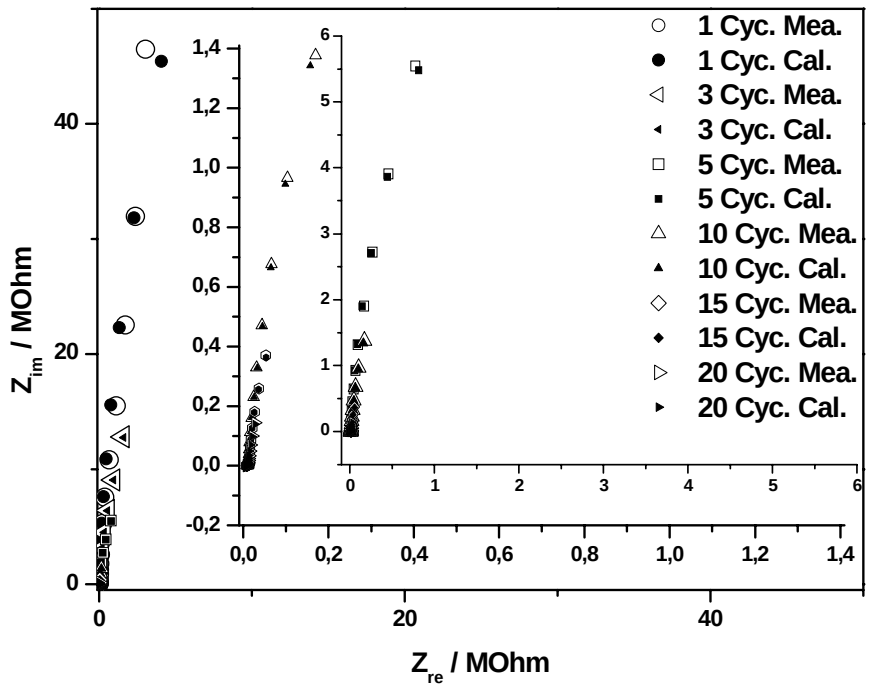

Figure 3.9 : Nyquist Plots of P(ProDOT-Bu_2) electrografted on SCFMEs correlated with the calculated data from theoretical equivalent circuit; R(C(R(Q(RW))))(C(R)).

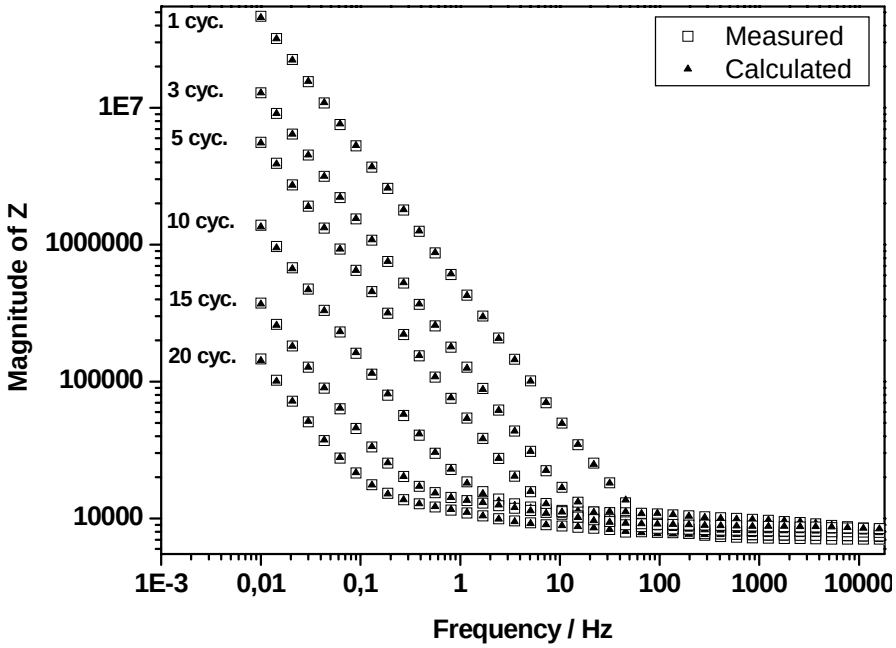

Figure 3.10 : Bode Magnitude Plots of P(ProDOT-Bu_2) electrografted on SCFMEs correlated with the calculated data from theoretical equivalent circuit; R(C(R(Q(RW))))(C(R)).

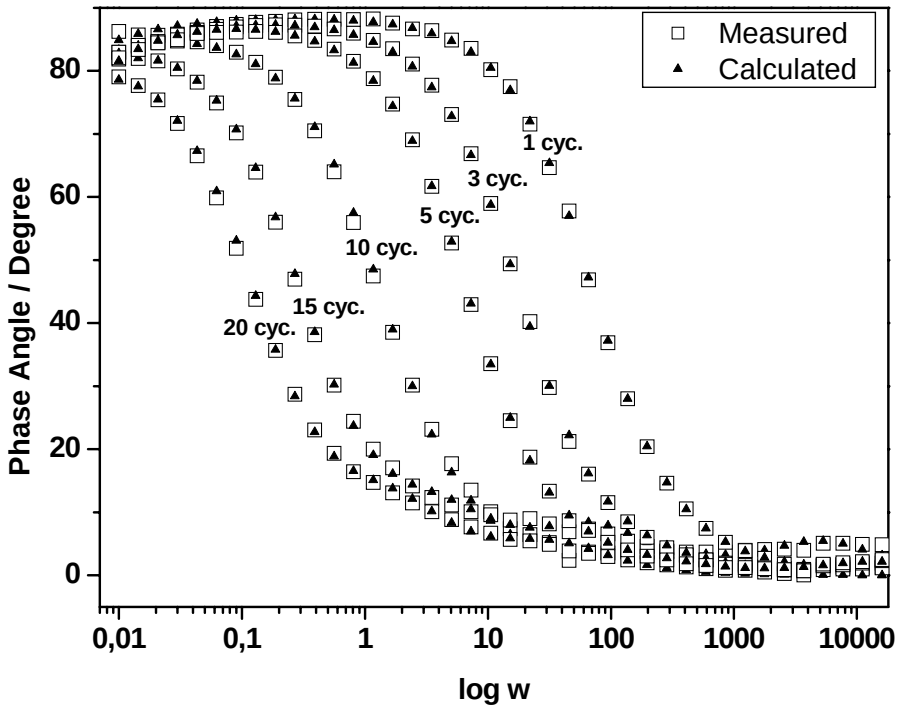

Figure 3.11 : Bode Phase Plots of P(ProDOT-Bu_2) electrografted on SCFMEs correlated with the calculated data from theoretical equivalent circuit; R(C(R(Q(RW))))(C(R)).

Table 3.1 : The variation of C_{LF} (from Nyquist at 10 mHz frequency) (Fig.3.11.) and phase angle (Fig.3.9) values of PProDOT-Bu_2 on SCFME.

Cycle Number	**1**	**3**	**5**	**10**	**15**	**20**
C_{LF} / $mFcm^{-2}$	1.36	4.95	11.02	45,89	177.45	446.13
Phase Ang./Deg.	87.3	86.4	85.2	83.6	81.8	79.9

*Carbon fiber Area: 25,12 x 10^{-5} cm^2

The electrochemical parameters of the SCFME/PProDOT-Bu_2 electrolyte system were evaluated by employing The ZSimpWin (version 3.10) software from Princeton Applied Research. We observed excellent agreement between experimental results and the parameters obtained from the best fitting electrical equivalent circuit model and the chi-squared (χ^2) values minimized to 10^{-4}. χ^2 is the function defined as the sum of the squares of the residuals. R(C(R(Q(RW))))(CR) equivalent circuit model simulated to find the optimum circuit conditions and compared. Electrical equivalent circuit was successfully applied to the experimental data to explain the interface between the carbon fiber microelectrode, and the polymer film for all cycles.

Model used during simulation is very similar to the models that we have reported recently in our previous work [73]. The first component is the bulk solution of solvent, R_s, is the parallel combination of the double layer capacitance C_{dl}, and R_1 is the charge transfer resistance. A series connection to charge transfer resistance (R_1) made up using CPE in parallel with R_2 where the the low frequency behavior is determined by the adsorption of cations and can be described by adsorption resistance and W is the Warburg impedance of the polymer. The last component is a capacitor element (C_{CF}) is introduced in parallel with a resistor (C_{CF}) correspondig to polymer coated carbon fiber capacitance and resistance (Figure 3.12).

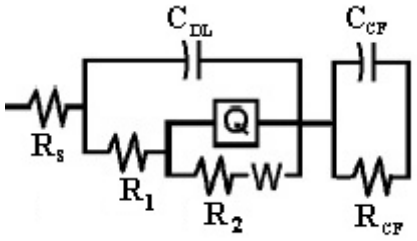

Figure 3.12 : Scheme of the equivalent circuit

Table 3.2 : Cycle dependence of the parameters calculated from the equivalent circuit which is given in Figure 3.8.

Cycle Number	**1**	**3**	**5**	**10**	**15**	**20**
R_s / kOhm	6.993	7.552	8.100	8.201	7.912	7.623
C_{dl} / µF	0.279	0.674	0.995	0.672	10.611	26.1
R_1 / kOhm	1260	2.14	0.961	1.68	5.44	5.37
Q / Y_0 / µSs^{-n}	5.04x 10^{-2}	0.42	1.69	10.42	29.82	75.92
n	0.883	0.957	0.968	0.964	0.967	0.951
R_2 /MOhm	832.123	67.245	49.006	24.213	5.088	2.521
W / Y_0 / µSs^{-n}	1.01x10^{-8}	6.22x10^{-14}	6.47x10^{7}	14.7	503	3.07
C_{CF} / µF	0.098	0.015	0.019	0.020	1.083	4.116
R_{CF} / kOhm	0.179	0.555	0.628	1.630	2.220	1.240
Chi Squared (χ^2)	**2.49x10^{-4}**	**1.15x10^{-4}**	**1.21x10^{-4}**	**6.46x10^{-4}**	**5.42x10^{-4}**	**3.50x10^{-4}**

Table 3.2. shows that suggested electrical equivalent circuit in this work was successfully applied to the experimental data to explain the increament of the capacitive behaviour of SCFME/PProDOT-Bu_2 with increasing the cycle number.

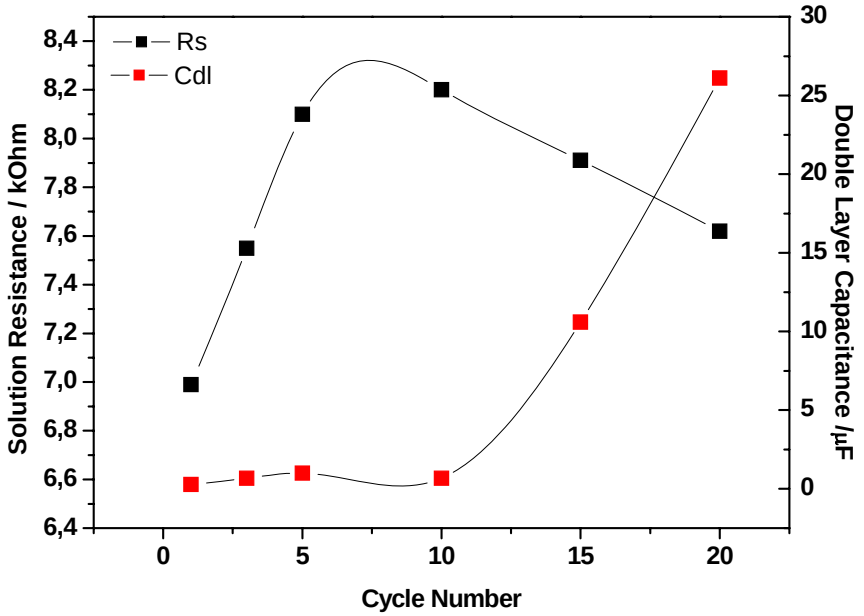

Figure 3.13 : Variation of solution resistance and double layer capacitance of the PProDOT-Bu_2 film with respect to the cycle number.

The variation of the solution resistance (R_s) and the double layer capacitance (C_{DL}) values were plotted with respect to the cycle number (Figure 3.12.). The solution resistance varies in a very narrow range around 8 kOhm while the double layer increases significantly as the cycle number increases after 10 cycles.

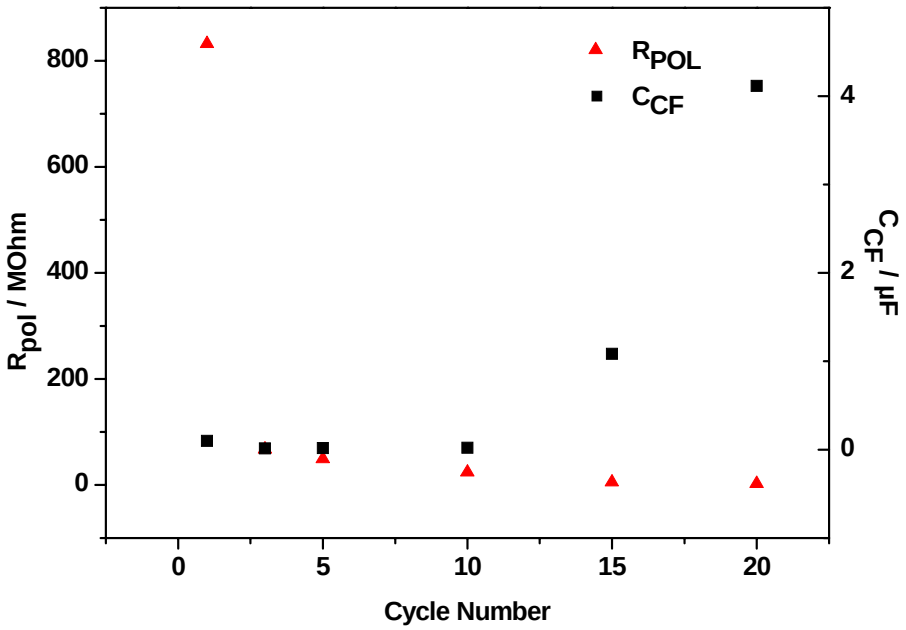

Figure 3.14 : Variation of polarization resistance and carbon fiber capacitance of the PProDOT-Bu_2 film with respect to the cycle number.

Additionally, the variation of the polarization resistance (R_P) and the carbon fiber capacitance (C_{CF}) values were plotted with respect to the cycle number (Figure 3.14). Both values are varies oppositely and carbon fiber resistance varies in a very narrow range around 4 μF which indicates the simulation data fits the experimental results perfectly.

3.1.3 FTIR Reflectance-Spectra (ATR-FTIR)

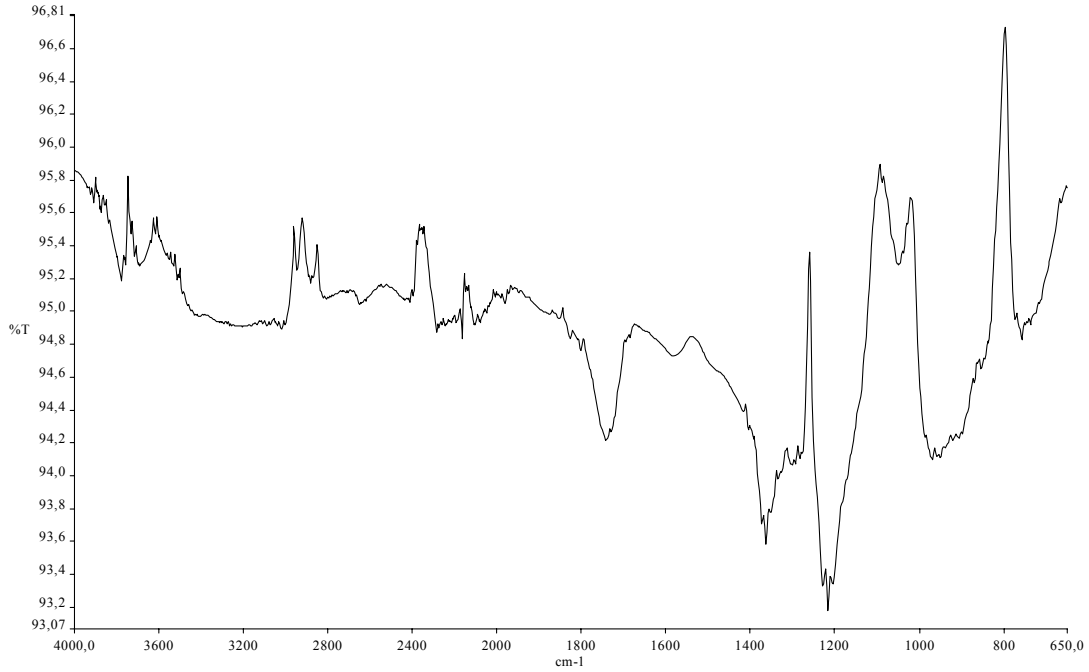

Figure 3.15.FTIR-ATR spectrum of CFMEs potentiodynamically coated by 10 mM ProDOT-Bu_2 at 100mV/s scan rate

FTIR-ATR of PProDOT-Bu_2 coated CFME shows the corresponding spectra between 4000 and 650 cm^{-1}. A pattern of five main bands (1470, 1287, 1155, doublet at 1017 and 826 cm^{-1}) was observed for a PProDOT-Bu_2 film coated on CFME Figure 3.15.

The band at 1470 cm^{-1} (aromatic stretching of C=C bond) and a peak at 1287 cm^{-1} (in plane deformation of C-H bond at β position) are known to be characteristic vibrational peaks of polythiophene. Vibrations at 1469-1470 cm^{-1}, 1295, 1286 cm^{-1} and 1160-1155 cm^{-1} originate from the stretching of C-C and C= C bonds in the thiophene ring.

Further vibrations from the C-S bond in the thiophene ring can be seen at 833-825 cm^{-1} assigned to ν(C-S) [C-S- stretching]. Vibrations at 1017-1048 cm^{-1} are assigned to stretching in the alkylenedioxy group [74].

3.1.4 Morphology of the films

Selections of CFs, coated with polymer under same conditions described above sections, were studied by SEM and AFM. All images shown represent an ex-situ microscopic work which allows us to determine the film deposition strategy on the SCFMEs.

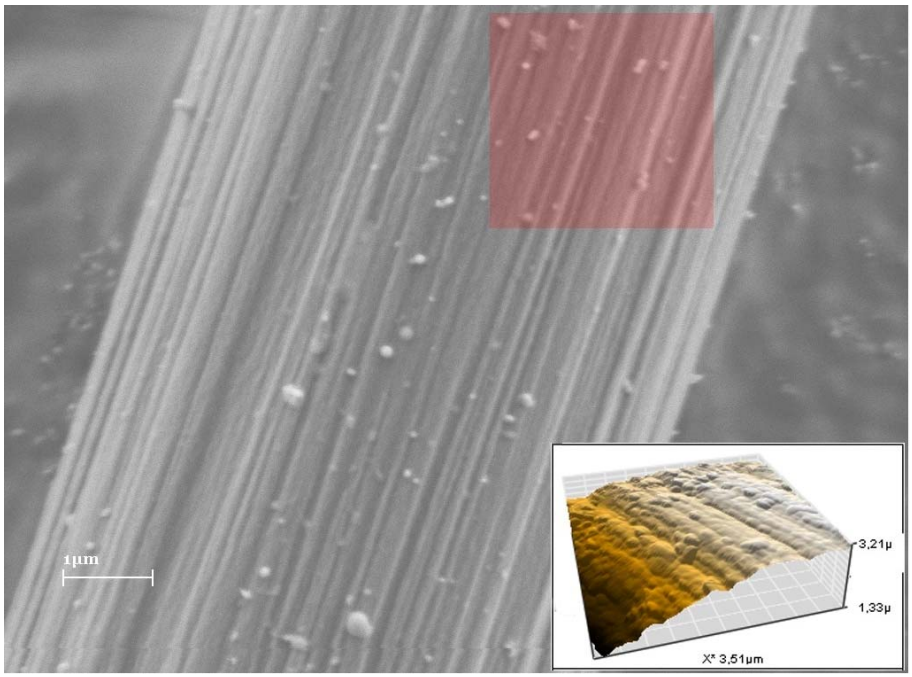

Figure 3.16 : SEM image of 1 cycle coated PProDOT-Bu_2 on SCFME. **Inset:** AFM images of PProDOT-Bu_2 coated CFME with image area of 3.5µm x 3.5µm.

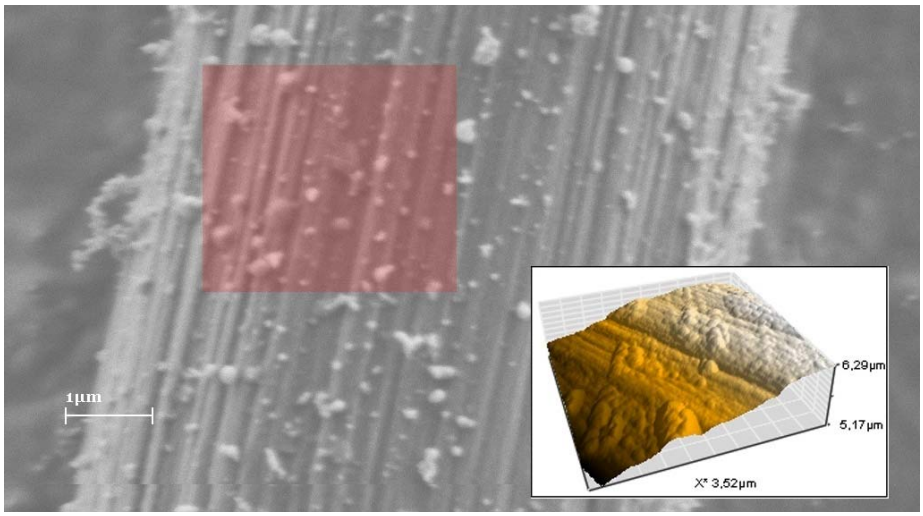

Figure 3.17 : SEM image of 3 cycles coated PProDOT-Bu_2 on SCFME. **Inset:** AFM image of PProDOT-Bu_2 coated SCFME with image area of 3.5µm x 3.5µm.

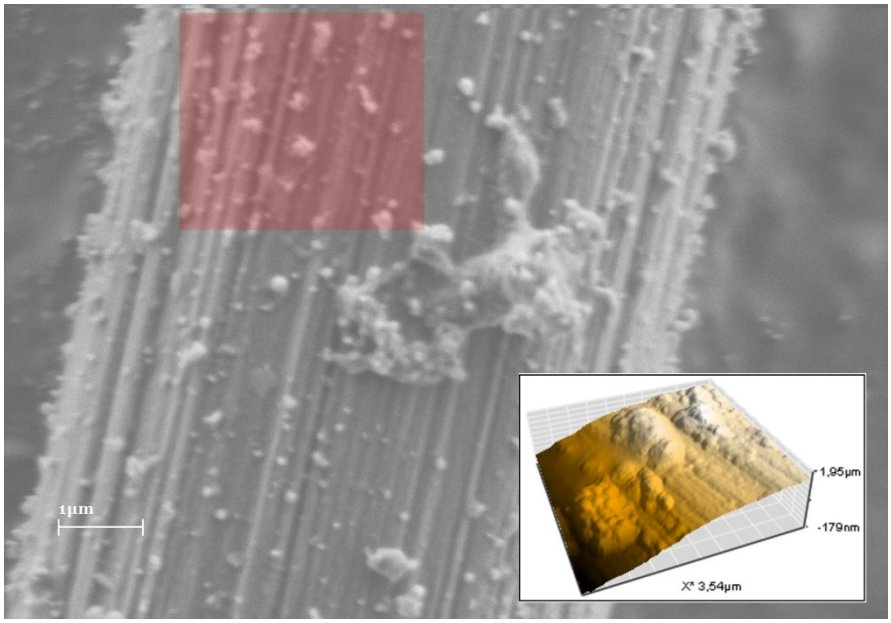

Figure 3.18 : SEM image of 5 cycles coated PProDOT-Bu_2 on SCFME. **Inset:** AFM images of PProDOT-Bu_2 coated SCFME with image area of 3.5µm x 3.5µm.

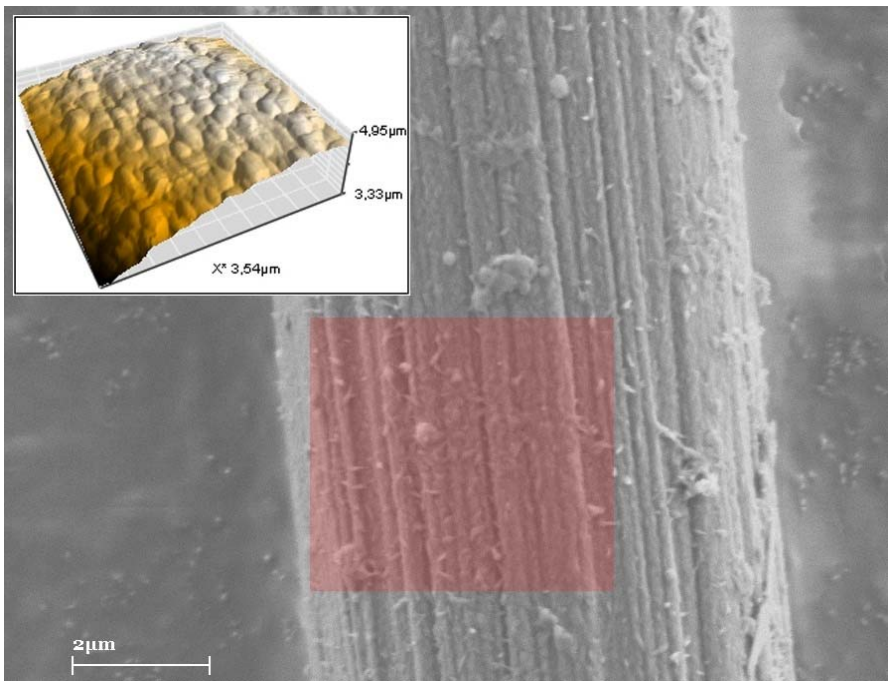

Figure 3.19 : SEM image of 10 cycles coated PProDOT-Bu_2 on SCFME. **Inset:** AFM images ofPProDOT-Bu_2 coated SCFME with image area of 3.5µm x 3.5µm.

Polymerization of PProDOT-Bu_2 starts both on the surface and in the striations of fiber at first cycle and continues up to third cycle with slighty disapperance of striations which is also another way to determine the second starting point of polymerization. With increasing the cycle number to five, local lumps are formed on the surface and the striations are sharply disappearing.

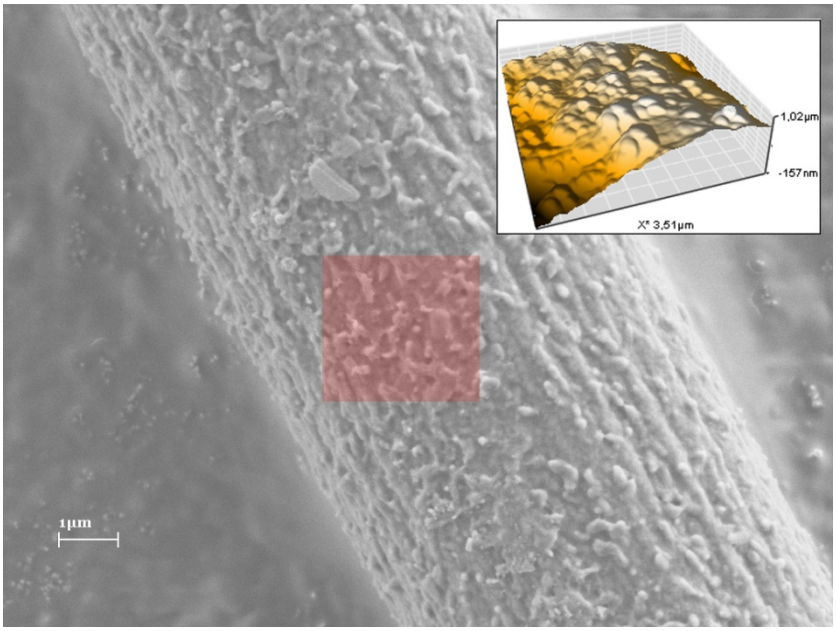

Figure 3.20 : SEM image of 15 cycles coated PProDOT-Bu_2 on SCFME **Inset:** AFM images of PProDOT-Bu_2 coated SCFME with image area of 3.5µm x 3.5µm.

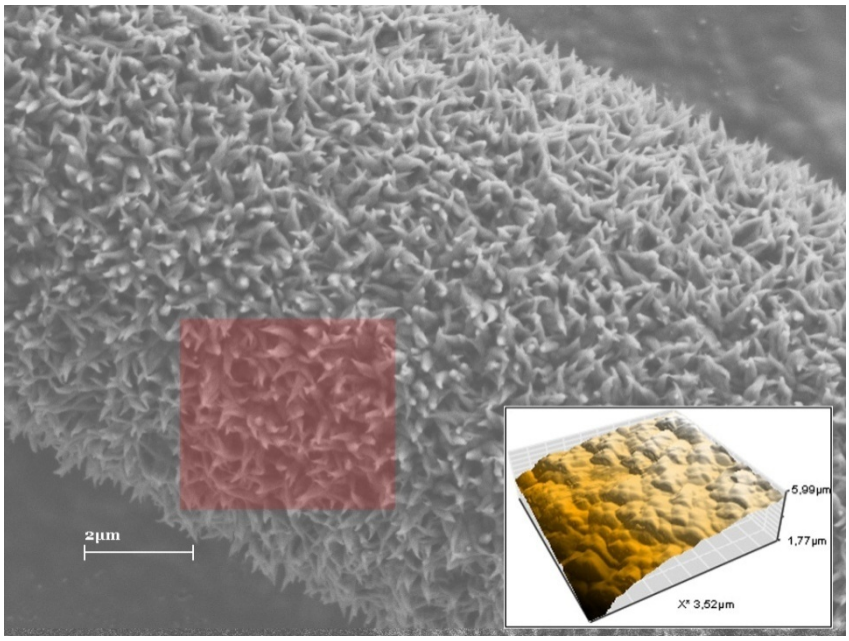

Figure 3.21 : SEM image of 20 cycles coated PProDOT-Bu_2 on SCFME **Inset:**AFM images of PProDOT-Bu_2 coated CFME with image area of 3.5µm x 3.5µm

In correlation, the reversible oxidation and reduction peaks of first 5 cycles are clearly seen and the amount of uncoated fiber area dominates the EIS results with slightly decreasing of phase angle and the magnitude of Z_{im} at nyquist plots. Also a monemer free plot of first five cycles obeys the adsorbtion mechanism with very reversible anodic and cathodic peaks due to thin film formation.

In contrast to unordered nucleation of first five cycles, all surface area of CF is coated with polymeric thin film after 10^{th} cycle and polymerization ratio increases.

Coating height, which causes a sharp increament of C_{dl} after 10^{th} cycle, shifts the redox couples negatively and positively at high scan rates in monomer free solutions due to bulk polymer film at interface with increasing porosity.

Film porosity can be explained when the 10^{th} 15^{th} and 20^{th} cycles are compared.The hillock like structures with app. equal Z ranges at 10^{th} cycle are becomes to hills via 15^{th} cyle. Finally after 20^{th} cycle, nanosize-villus like porous surface with a very large surface area obtained.

3.2 Potential Effects on PProDOT-Bu_2 coated SCFMEs; an EIS Investigation at Applied Potentials

PProDOT-Bu_2 film deposited at 100 mV/s, 20 cycle in 0.1 M $NaClO_4$/ACN solution and electrochemical impedance spectroscopy (EIS) measurements were performed at different applied potentials in the range of 0.1 V to 1.3 V with a potential step of 0.1V in parallel to cyclic voltammogram of the PProDOT-Bu_2 in monomer free electrolyte solution where stability of the film exhibit electroactivity up to 0.8 V potential applied. The film morphology dramatically changes and surface area decreases when the applied potential arises around 1.2 V.

3.2.1 EIS and Equivalent Circuit Modelling of PProDOT-Bu_2 on SCFMEs

Figures 3.22 and 3.23 show bode phase angle and magnitude of Z plots in which the frequency dependence of the system is clearer compared to Nyquist plot (Figure 3.21.). In the potential region as the frequency increase from 10 mHz to 10 Hz magnitude of impedance exhibits a large drop, in the case of higher electrode potentials drop in magnitude is a narrow frequency window 10 mHz to 1000 Hz. From these observations we can conclude that the most capacitive film obtained when the 0.4 V potential applied.

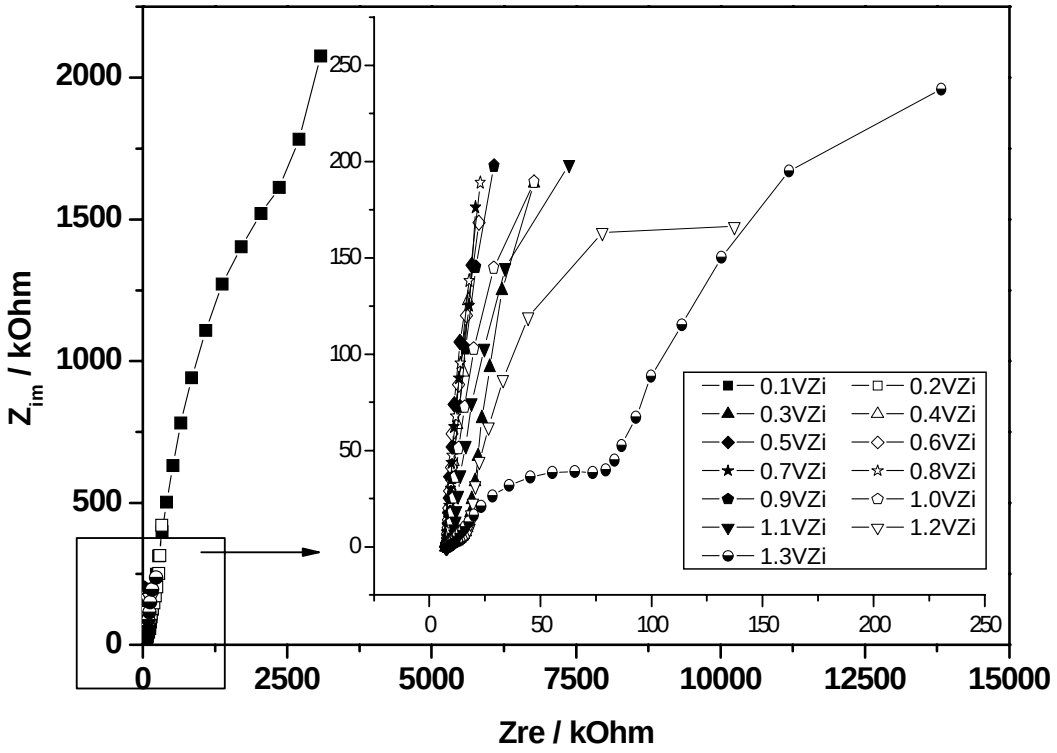

Figure 3.22 : Nyquist plots at -0.1 V to 1.2 V for a PProDOT-Bu_2 film deposited at 100 mV/s, 20 cycle in 0.1 M $NaClO_4$/ACN solution.

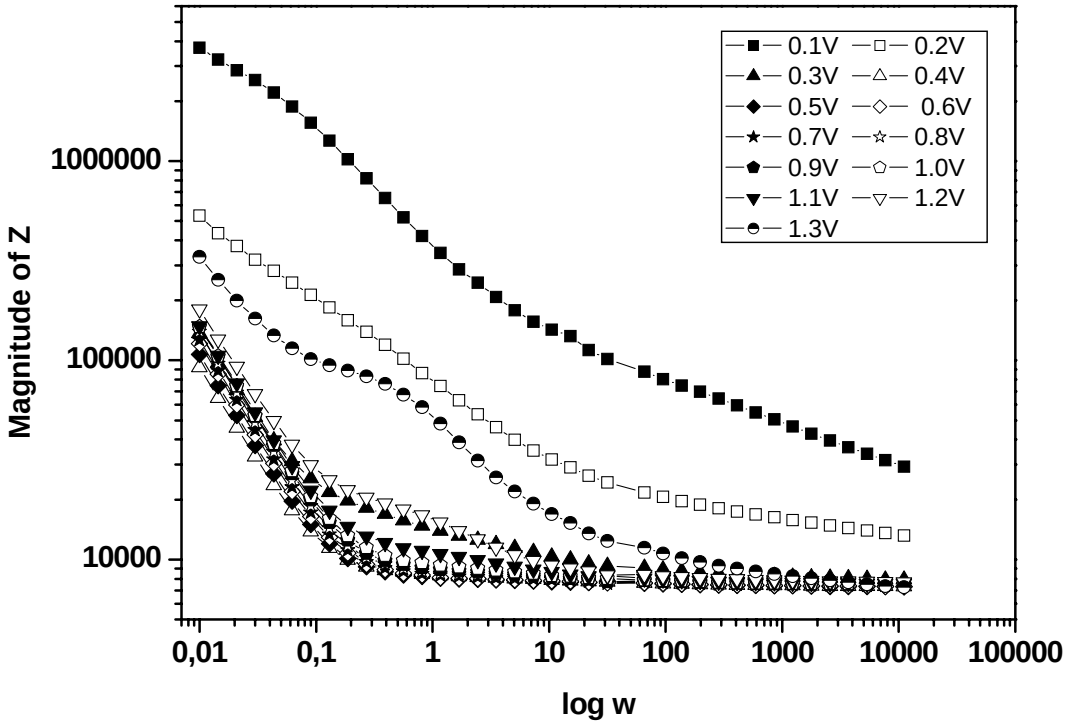

Figure 3.231 : Bode plots at 0.1 V to 1.2 V for a PProDOT-Bu_2 film deposited at 100 mV/s, 20 cycle in 0.1 M $NaClO_4$/ACN solution.

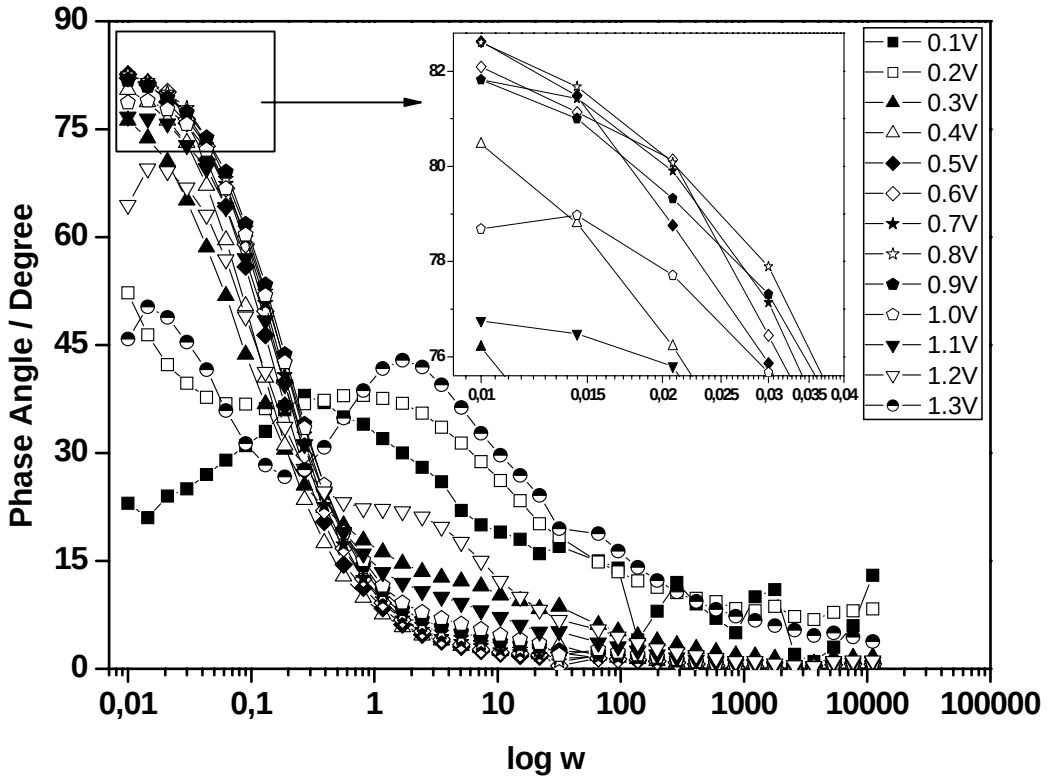

Figure 3.24 : Bode phase angle plots at 0.1 V to 1.2 V for a PProDOT-Me_2 film deposited at 100 mV/s, 20 cycle in 0.1 M $NaClO_4$/ACN solution.

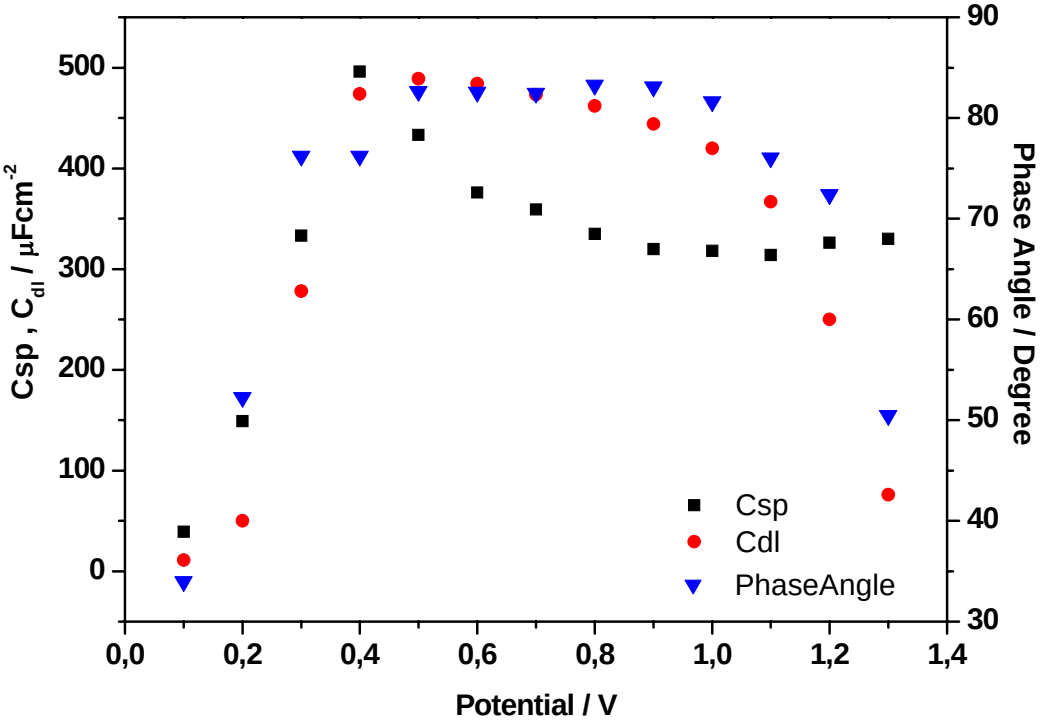

Figure 3.25 : Variation of low frequency and double layer capacitances with the low frequency phase angle points at applied potentials of the PProDOT-Bu_2 film.

Bode phase angle of the films was given in Figure 3.23. We can separate into three frequency regions namely low, medium and high frequency regions.

Low frequency region is from 10 mHz to 1 Hz, in this regions all potential except 0.1V, 0.2V, 1.2V and 1.3 V, polymer film shows a maximum at 10 mHz with a phase angle of around (-80^{o}), starting from this frequency phase angle decreases and where the electrode behaves in the low frequency region of 100 to 200 mHz, at 1.3 V two peak observed at 10 mHz (-45^{o}) and 1 Hz (-40^{o}).

Figure 3.25 also illustrates the variation of the low frequency capacitance values of PProDOT-Bu_2 film deposited electrochemically at 100 mV/s, 20 cycle in 0.1M $NaClO_4$/ACN solution. The shape of the plot has a very good agreement with the corresponding CV of the polymer film in monomer free solution up to 1.3 V.

After 1.2V applied to the system, the low frequency values decreases dramatically with respect to the double layer capacitance values as shown in Figure 3.25.

The low frequency capacitance values from impedance spectroscopy were obtained from the slope of a plot of the imaginary component (Z_{IM}) of the impedance at low frequencies versus inverse of the reciprocal frequency (f) using previously described equation (1-3).

Table 3.3: Potential dependence of the parameters calculated from the model which is given Figure 3.10.

	0.1V	**0.2V**	**0.3V**	**0.4V**	**0.5V**	**0.6V**
R_s / kOhm	16.22	12.61	8.25	7.47	7.38	7.39
C_{dl} / µF	$4.85x10^{-4}$	$1.15x10^{-2}$	14.16	54.58	52.79	$3.55x10^{9}$
R_1 /kOhm	16.26	3.73	8.08	1.83	1,67	1.28
Q / Y_0 / Ss^{-n}	$1.06x\ 10^{-7}$	$4,97x10^{-6}$	$5,63x10^{-5}$	$5.89x10^{-5}$	$4.57x10^{-5}$	$5.18x10^{-5}$
n	0.66	0.55	0.91	0.98	0.98	0.97
R_2/MOhm	0.05	0,40	7.13	$1.00x10^{-7}$	0.18	1.25
W / Y_0 / Ss^{-n}	$1.37x10^{-6}$	$9.61x10^{-6}$	6.32	$3.08x10^{-6}$	$1.95x10^{-6}$	$2.64x10^{-6}$
C_{CF} / µF	2.13	46.95	1.96	5.96	4.58	3.45
R_{CF} / kOhm	998.31	7720.87	2.65	0.51	0.36	0.34
Chi Squared (χ^2)	**$5.31x10^{-4}$**	**$6.77x10^{-4}$**	**$1.02x10^{-4}$**	**$8.00x10^{-5}$**	**$9.58x10^{-5}$**	**$8.02x10^{-5}$**

Table 3.3 continue

	0.7V	**0.8V**	**0.9V**	**1.0V**	**1.1V**	**1.2V**
R_s / kOhm	7.42	7.44	7.53	7.53	7.62	7.71
C_{dl} / µF	25.76	21.93	16.29	15.58	12.54	8.11
R_1 / kOhm	1.08	1.27	1.44	2.06	3.59	11.49
Q / Y_0 / Ss^{-n}	$5.71x10^{-8}$	$5.33x10^{-5}$	$5.38x10^{-5}$	$5.28x10^{-5}$	$5.39x10^{-5}$	$4.84x10^{-5}$
n	0.97	0.97	0.97	0.96	0.95	0.97
R_2 /MOhm	0.87	1.13	0.56	0.76	1.09	0.44
W / Y_0 / Ss^{-n}	$1.91x10^{-6}$	$1.53x10^{-6}$	$2.19x10^{-6}$	$5.15x10^{-6}$	$1.66x10^{-5}$	$1.27x10^{-4}$
C_{CF} / µF	3.24	3.11	3.15	2.84	3.34	3.71
R_{CF} / kOhm	0.28	0.34	0.35	0.49	0.79	1.61
Chi Squared (χ^2)	**$7.55x10^{-5}$**	**$9.98x10^{-5}$**	**$1.25x10^{-4}$**	**$2.03x10^{-4}$**	**$2.22x10^{-4}$**	**$1.48x10^{-4}$**

The electrochemical parameters of the SCFME/PProDOT-Bu_2 electrolyte system were evaluated by employing The ZSimpWin (version 3.10) software from Princeton Applied Research.

We observed excellent agreement between experimental results and the parameters obtained from the best fitting electrical equivalent circuit model and the chi-squared (χ^2) values minimized to 10^{-4}. $\chi 2$ is the function defined as the sum of the squares of the residuals.

Same equivalent circuit model (Figure 3.12.) was simulated to find out the optimum circuit conditions and compared. Electrical equivalent circuit was successfully applied to the experimental data of applied potentials between 0.1 V and 1.2 V to explain the interface between the carbon fiber microelectrode, and the polymer film for all cycles at applied potentials.

Due to change in surface morphology (will be explained in next section), 1.3 V applied system could not be simulated perfectly and the chi-squared values obtained above 10^{-4}.

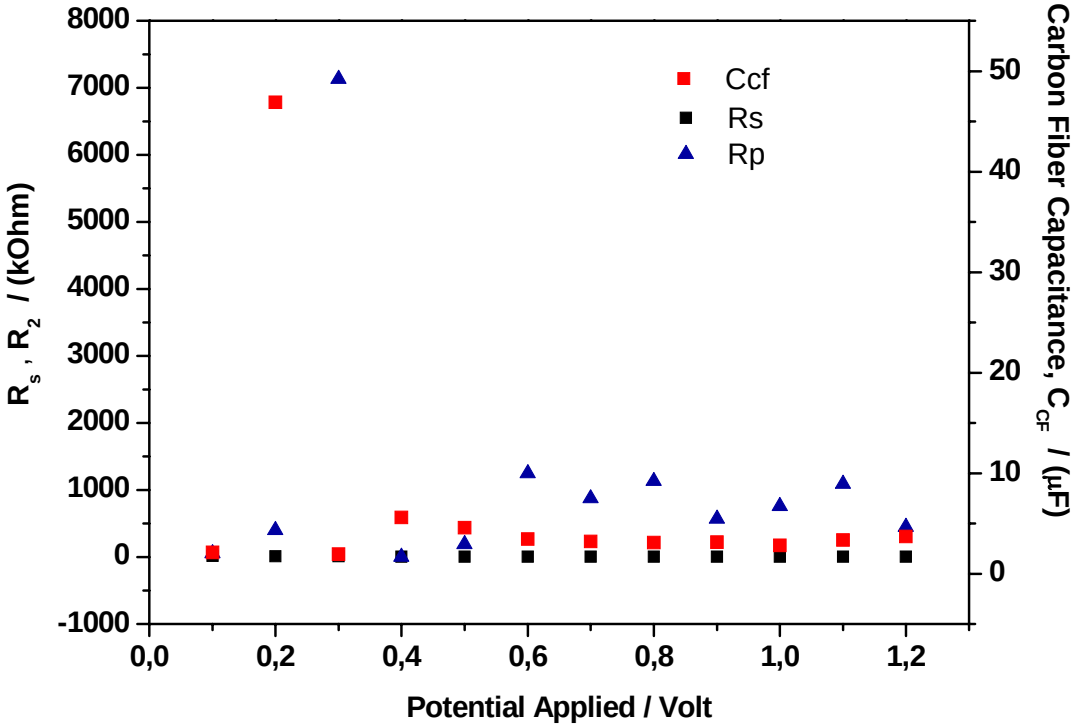

Figure 3.26 : Variation of the solution and polarization resistance, double layer capacitance of the PProDOT-Bu_2 film.

Figure 3.26 shows variation of solution resistance, double layer capacitance and R_2 of the PProDOT-Bu_2 film. Rs is almost constant and it is independent of E_{dc}.

With comperasion of Table 3.2 and Table 3.3 ,experimental results allow us to describe R_s as the solution, R_{CF} as the carbon fiber and R_2 as the adsorption resistance while the C_{CF} as the coated carbon fiber capacitance.

3.2.2. Morphology of Coatings

According to experimental EIS results and theoretical equivalent circuit simulations, the dramatic decrease of double layer capacitance can be easily explained with the help of SEM micrographs.

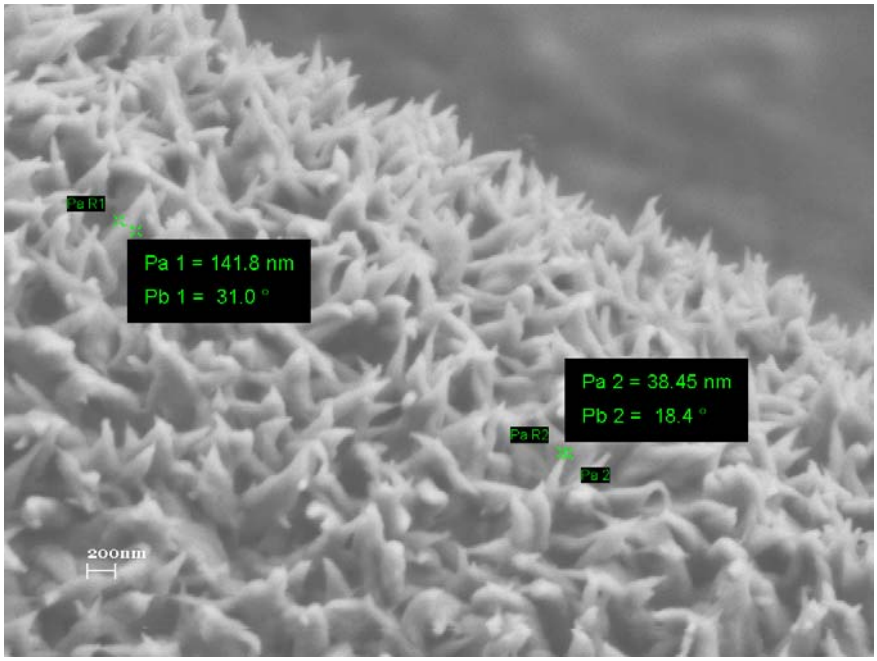

Figure 3.27 : SEM image of 20 cycles coated PProDOT-Bu_2 on SCFME after 0.8V potential applied.

Figure 3.28 : SEM image of 20 cycles coated PProDOT-Bu_2 on SCFME after 1.2 V potential applied

Selections of CFs, coated with polymer under same conditions described above sections, were studied by SEM at two of applied potentials.Figure 3.27 and 3.28 corresponds to the films surfaces of 0.8 V and 1.2 V respectively.

The surface morphology of the thin films does not change significiantly up to 0.8 V potential applied.

But the nano-villus like structures of the films surprisingly disappears after that potential and non-porous surface results with the decrease of the surface area of the film after 1.2 V potential applied.

In correlation, the surface of the film shown in Figure 3.28 is resulted with the decreasing double layer capacitance or low frequency phase angle obtained from EIS results.

In addition, experimental results could not be simulated at high potentials. This may be another sign for changing film porosity where the suggested equivalent circuit fits to he experimental data at only porous surfaces as suggested in literarure [74].

3.3 Capacitive Behavior of PProDOT-Bu_2 Thin Films on Different Substrates

Electropolymerization processes were performed in 0.1 M $NaClO_4$/ACN with 10 cycles for Pt and ITO coated glass substrates in order to investigate electrochemical impedance results such as double layer capacitance and low frequency capacitance. Obtained results were compared with EIS results of bare substrates ACN was chosen as a standart solvent to prepare electrolyte for 0.01 M ProDOT-$(Bu)_2$ solution during this study. Electropolymerization of ProDOT-$(Bu)_2$ / SCFMEs is previously showed in Figure 3.7.

3.3.1 Electropolymerization of PProDOT-Bu_2 on SCFME, Pt and ITO Surfaces

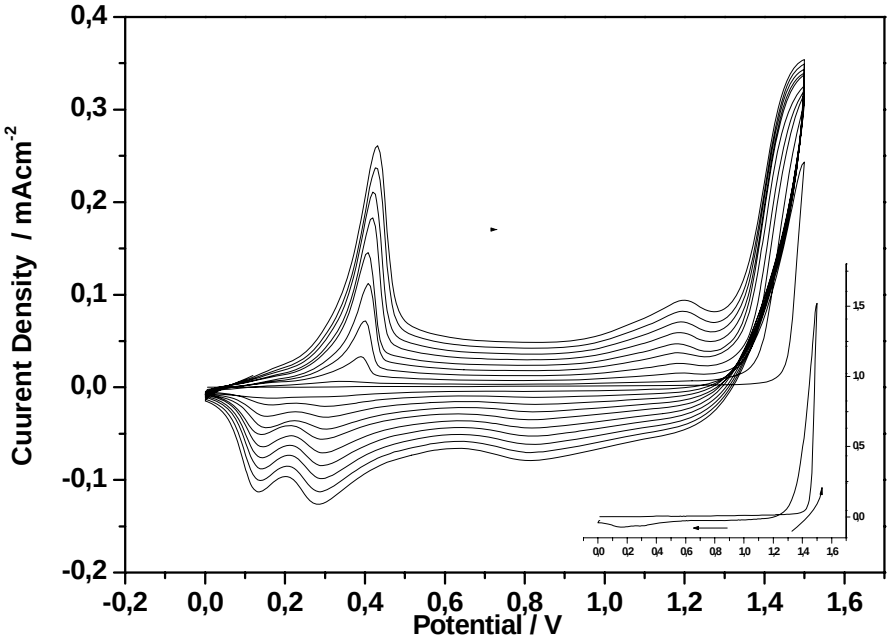

Figure 3.29 : Cyclic voltammetry of electrogrowth of 10^{-2} M ProDOT$(Bu)_2$ in 0.1 M $NaClO_4$/ACN on Pt surface; scan rate: 100 mV/s.Inset: First cycle of ProDOT$(Bu)_2$ on Pt surface.

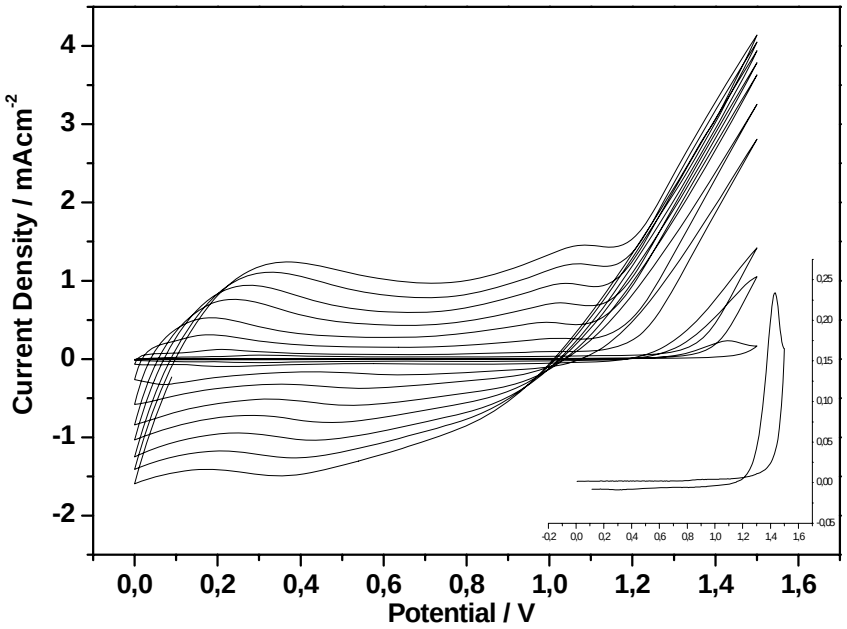

Figure 3.30 : Cyclic voltammetry of electrogrowth of 10^{-2} M ProDOT$(Bu)_2$ in 0.1 M $NaClO_4$/ACN on ITO coated glass surface; scan rate: 100 mV/s. Inset: First cycle of ProDOT$(Bu)_2$ on ITO coated glass surface.

Cyclic voltammograms of ProDOT-Bu_2 films in 0.1 M $NaClO_4$/ACN on ITO coated glass and Pt surfaces are shown in Figure 3.29 and 3.30 where the characteristic oxidation and reduction peaks are clearly seen around 0.4V and 1.2V as excepted.

3.3.2 Comperative EIS Study of PProDOT-Bu_2 on SCFME, Pt and ITO Surfaces

EIS results of the films are plotted in Figures 3.31, 3.32 and 3.33. Vertical shift of the graphs in the Bode plot is a sign of changing solution resistance which is dominantly related with the distance of electrodes and electrode geometry as well.

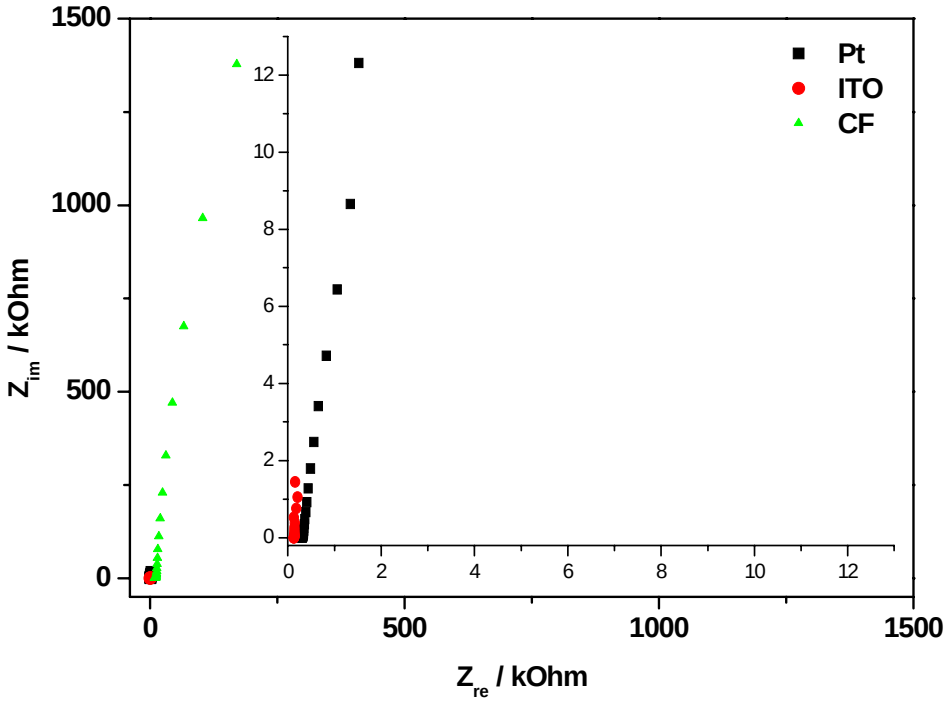

Figure 3.31 : Nyquist plots of PProDOT-Bu_2 film deposited at 100 mV/s, 10 cycle in 0.1 M $NaClO_4$/ACN on SCFME, Pt and ITO coated glass substrates.

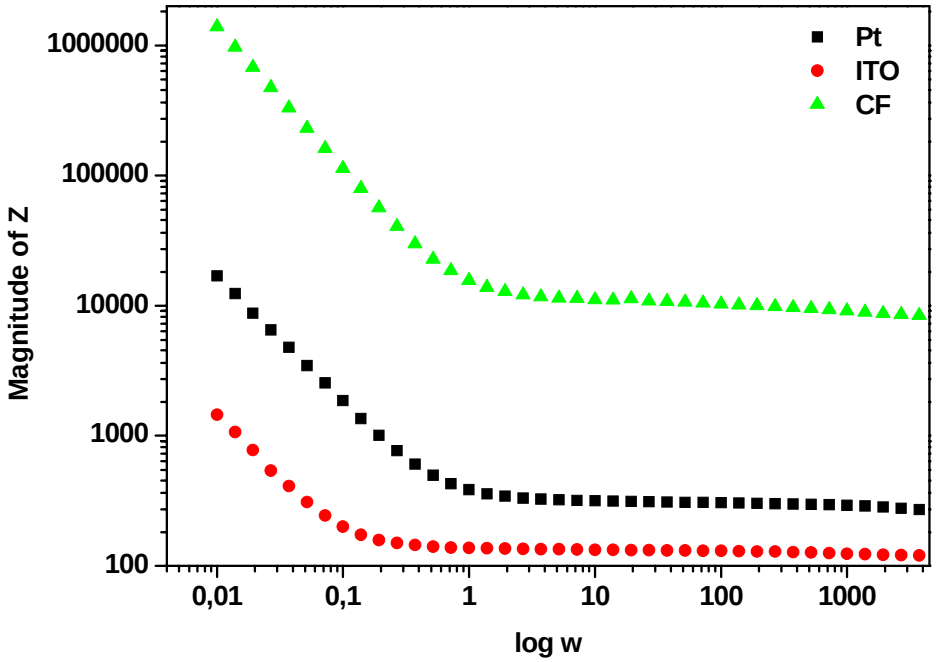

Figure 3.32 : Bode plots of PProDOT-Bu_2 film deposited at 100 mV/s, 10 cycle in 0.1 M $NaClO_4$/ACN on SCFME, Pt and ITO coated glass substrates.

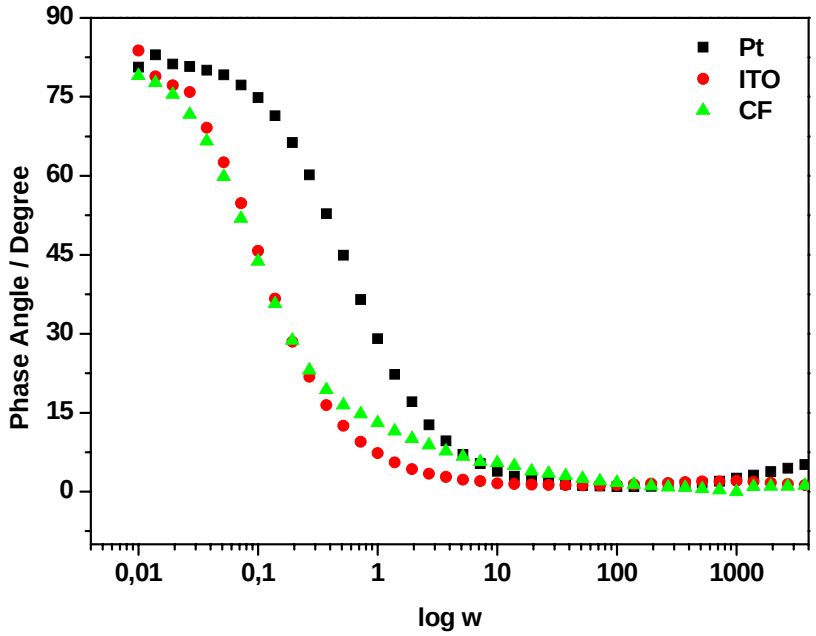

Figure 3.33 : Bode phase plots of PProDOT-Bu_2 film deposited at 100 mV/s, 10 cycles in 0.1 M $NaClO_4$/ACN on SCFME, Pt and ITO coated glass substrates.

C_{dl} and C_{LF} values of all substrates were calculated for coated and uncoated (graphs are not shown) substrates as described above and summarized in Tables 3.4 and 3.5.

Table 3.4 Double layer and low frequency capacitance values of bare ITO coated glass, Pt and SCFME in 0.1 M $NaClO_4$/ACN solutions.

BARE	C_{LF} / mFcm^{-2}	C_{dl} / mFcm^{-2}
ITO	22 x 10^{-3}	9.43 x 10^{-2}
Pt	3,9	1.54
CF	2.21x10^{-2}	1.26 x 10^{-1}

Table 3.5 Double layer and low frequency capacitance values PProDOT-Bu_2 film deposited at 100 mV/s, 10 cycles in 0.1 M $NaClO_4$/ACN on SCFME, Pt and ITO coated glass substrates.

10 cyc	C_{LF} / mFcm^{-2}	C_{dl} / mFcm^{-2}
ITO	8.85	6.45
Pt	83.52	164.41
CF	45.32	272.34

Table 3.6 Ratios of double layer and low frequency capacitance values of SCFME, Pt and ITO coated glass substrates.

	$C_{LF\ coated/uncoated}$	$C_{dl\ coated/uncoated}$
ITO	402	68
Pt	21	106
CF	2036	2142

The C_{dl} and C_{LF} ratios of all substrates for coated and uncoated substrates. (Table 3.6.) Indicates an increament when coated with thin films of ProDOT-Bu_2. However, depending on the substrates, Pt favors the increament of Cdl and ITO coated glass favors an increament of C_{LF} while SCFME favours the both values nearly equal with an increasing ratio of more than 2000 times as compared to bare SCFME.

4. CONCLUSION

2,2-Dibutyl-3,4-propylenedioxythiophene monomer was performed onto single carbon fiber micro electrode by electrochemical polymerization and electrochemical characterizations, morpholology of the films were studied. Testing the polymer film in the use on SCFME as an active electrode material in supercapacitor applications was tested at different potentials.

Electrochemical Impedance Spectroscopy is a powerful tool for the analysis of electrochemical system. This technique was used to explain electrochemical characteristics of the polymer electrodes like resistance, capacitance and impedance. Equivalent circuit simulations corresponding to the polymer modified microelectrodes calculated and suggested values of the each component was found aggrements with experimental data.

Device properties based on PProDOT-Bu_2 were checked with the applying potentials. Typical CV of the polymeric film exhibits very well-defined and reversible redox processes. The impedance study on specific capacitance values investigated between 0.1 V and 1.4 V. A potential value of 0.4 V was found to be the most suitable condition for the polymer modified microelectrodes as supercapacitor components.

Morphology of the resulting polymer shows that thickness of the polymer film is a function of number of cycles and increases with the number of deposition charge during the electropolymerization. Morhology of the film also changes during applying potential which also detoriates both the film surface and the capacitive behavior of film.

Investigation of out different substares such as Pt, ITO coated glass showed that, SCFMEs are the most suitable ones for using supercapacitor components in comparasion with to other 10 cycles of composite electrodes.

5. REFERENCES

[1]**Diaz, A.F., Kanazawa, K.K. and Gardini, G.P.,** 1979. Electrochemical polymerization of pyrrole, *J.Chem.Soc.*Chem.Commun.*,* **14**, 635-636.

[2]**Nalwa, H.S.,** 1997. Handbook of Organic Conductive Molecules and Polymers, vol.1-4, Wiley, Chichester, UK.

[3]**Skotheim, T.A., Elsenbaumer, R.L. and Reynolds, J.R.,** 1998. Handbook of Conducting Polymers, 2nd ed., Marcel Dekker, New York.

[4]**Storsberg, J., Ritter, H., Pielartzik, H. and Groenendaal, L.,** 2000. Cyclodextrins in polymer synthesis: Supramolecular cyclodextrin complexes of pyrrole and 3, 4-ethylenedioxythiophene and their oxidative polymerization, *Adv.Mater*., **8**, 567-569.

[5]**Inzelt, G., Pineri, M., Schultze, J.W. and Vorotyntsev, M.A.** 2000. Electron and proton conducting polymers: Recent development and prospects, *Electrochim.Acta*, **45,** 2403.

[6]**Heeger, A.J.** 2001. Semiconducting and metallic polymers: The fourth generation of polymeric materials, *J.Phys.Chem.B*., **105,** 8475.

[7]**Ateş M.,** Electropolymerization and Characterization of Carbazole Based Polymers on Carbon Fiber Microelectrodes, Electrochemical Impedance Spectroscopy, and Sensor Behaviors Against Dopamine, *PhD Thesis,* İ.T.Ü. Instute of Science and Technology, İstanbul

[8]**Hepburn, A.R., Marshall, and Maud J.M,** 1991. Novel electrochromic films via anodic-oxidation of carbazolyl substituted polysiloxanes, *Synth.Met.,* **43**, 2935.

[9]**Yamamoto, T.J.,** 1981. Conjugated Polymers with Electronic and Optical Functionalities: Preparation by Organometallic Polycondensation, Properties, and Applications, *J.Chem.Soc.Chem.Commun.,* **187**, 226.

[10]**Mastragostino, M., Marinangeli, A.M., Corradini, A. and Giarcobbe, S.,** 1989. Conducting polymers as electrochromic materials*, Synth.Met.,* **28,** 1**,** C501-C506.

[11]**Dubois, J.C., Sagnes O and Henry F,** 1989. Polyheterocyclic conducting polymers and composites derivates, *Synth.Met.,* **28,** C871-C878.

[12]**Roncali, J., Garreau, R., Delabouglise, D., Garnier, F. and Lemaire, M.,** 1989. Modification of the structure and electrochemical properties of poly(thiophene) by ether groups, *J.Electroanal.Chem.,* **269**, 337-349.

[13]**Saleneck, W.R.,** 1991. Science and applications of conducting polymers, proc of the 6th Europhysics Industrial workshop, Adam Hilger

[14]**Bradley, D.D.C.** 1991. Molecular electronics-aspects of the physics, *Chemistry in Britain*, **27**, 719-723.

[15]**Davidson**, **K.,** 1991. Application of density functional theory in the synthesis of electroactive polymers, *Educ.Chem*., **28**, 155.

[16]**Doblhofer, K. and Rajeshwar**, **K,** 1998. *Handbook of Conducting Polymers* , 531.

[17]**Feast, W.J., Tsibouklis, J., Pouwer, K.L., Groenendaal, L. and Maijer, E.W.,** 1996. Synthesis, processing and material properties of conducting polymers, *Polymer,* **37,** 5017.

[18]**Schopf, G. and Kobmehl, G.,** 1997. Polythiophene-Electrically conductive polymers, *Adv.Polym.Sci.,* **129**, 3-145.

[19]**Skotheim, T.A., Reynolds, J.R. and Elsenbaumer, R.L.,** Handbook of Conducting Polymers, 2nd Ed.; Eds., Marcel Dekker, New York, 1997.

[20]**Gorman, C.B. and Grubbs, R.H.,** Conjugated Polymers: The novel science and technology of conducting and nonlinear optically active materials, , Kluwer Academic Publishers, Dordrecht, The Netherlands, 1992, 1.

[21]**Elsenbaumer, R.L., Jen, K.Y. and Oboodi, R.,** 1986. Processable and environmentally stable conducting polymers, *Synth. Met.,* **15**, 169.

[22]**Sato, M., Tanaka, S. and Kaeriyama, K.,** 1986. Soluble Conducting polythiophenes, *J. Chem. Soc., Chem.Commun.,* **11**, 873.

[23]**Yoshino, K., Gu and H.B.,** 1986. Effect of ammonium gas on electrical property of conducting polymers, *Japanese J.Appl.Phys.Part I.* Regular papers notes and review papers, **25**, 1064.

[24]**Hotta, S., Rughooputh, D.D.V., Heeger, A.J. and Wudl, F.,** 1987. Spectroscopic studies of soluble poly(3-alkylthienylenes), *Macromolecules,* **20**, 212.

[25]**Roncali, J., Garreau, R., Yassar, A., Marque, P., Ganier, F. and Lemaire, M.,** 1987. Effects of steric factors on the electrosynthesis and properties of conducting poly(3-alkylthiophenes), *J.Phys.Chem.*, **91,** 6706.

[26]**Bryce, M.R., Chissel, A., Kathirgamanathan, P., Parker, D. and Smith, N.M.R.,** 1987, Soluble conducting polymers from 3-substituted thiophenes and pyrroles, *J. Chem. Soc. Chem. Commun.,* **6**, 466.

[27]**X. Ren, P.G. Pickup**, 1997. Impedance measurements of ionic conductivity as a probe of structure in electrochemically deposited polypyrrole films *J. Phys. Chem.*, **97**, 5356.

[28]**Gençtürk A.,** 2006. Electropolymerization and characterization of 1-4-methylphenyl-1H- pyrrole and 2,2- dimethylpropylenedioxy thiophene *MSc Thesis,* İ.T.Ü. Instute of Science and Tech., İstanbul

[29]**M. Leclerc, G. Daoust, J. Chem. oc**. 1990. Desing of New Conducting 3,4-Disubstitited Polythiophenes *Journal of the Chemical Society-Chemical Communications*, **3**, 273.

[30]**L. B. Groenendal, F. Jonas, D. Freitag, H. Pielartzik, J. R. Reynolds,** 2000. *Advanced Materials.* Poly(3,4-ethylenedioxythiophene) and Its Derivatives, **12**, 481.

[31]**G. Tourillon, F. Garnier,** 1984. Structural effect on the electrochemical properties of polythiophene and derivatives*Journal of Electroanalytical. Chemistry,* **161,** 51. .

[32]**M. Dietrich, J. Heinze, G. Heywang, F. Jonas**, 1994. Electrochemical and Spectroscopic Characterization of Polyacetylenedioxythiophenes, *Journal* of *Electroanalitical Chemistry*, **369,** 87.

[33]**S. A. Sapp, G. A. Sotzing, J. R. Reynolds,** 1998. High contrast ratio and fast-switching dual polymer electrochromic devices *Chemistry of. Materials*, **10,** 2101.

[34]**A.Kumar, D. M. Welsh, M. C. Morvant, F. Piroux, K. A. Abboud, J. R. Reynolds,** 1998. Conducting poly(3,4-alkylenedioxythiophene) derivatives as fast electrochromics with high-contrast ratios *Chemistry of Materials*, **10,** 896.

[35]**E. Havinga, C. M. Mutsaers, L. W. Jenneskens,** 1996. Absorption Properties of Alkoxy-Substituted Thienylene-Vinylene Oligomers as a Function of the Doping Level, *Chemistry of. Materials*, **8,** 769.

[36]**L. Groenendaal, G. Zotti, F. Jonas**, 2001. Optical, conductive and magnetic properties of electrochemically prepared alkylated poly(3,4-ethylenedioxythiophene)s, *Synthetic Metals***. 118,** 105.

[37] **C. L. Gaupp, D. M. Welsh, J. R. Reynolds,** 2002. Poly(ProDOT-Et_2): A High-Contrast, High-Coloration Efficiency Electrochromic Polymer *Macromoleculer Rapid Communications*, **23,** 885.

[38]**D. M. Welsh, L. J. Kloeppner, L. Madrigal, M. R. Pinto, K. S. Schanze, K. A. Abboud, D. Powell, J. R. Reynolds**, 2002. Regiosymmetric Dibutyl-Substituted Poly(3,4-propylenedioxythiophene)s as Highly Electron-Rich Electroactive and Luminescent Polymers *Macromolecules*, **35**, 6517.

[39]**L.Groenendal, Gianni Zotti, Pierre-Henri Aubert, Shane M. Waybright, John R. Reynolds,** 2003. Electrochemistry of poly(3,4-alkylenedioxythipohene) derivatives.*Advanced Materials* , **15**, 855.

[40]**Aricò, A. S., P. Bruce, et al.** 2005. Nanostructured materials for advanced energy conversion and storage devices. *Nature Materials*, **4,** 366.

[41]**Burke, A.** 2000. Ultracapacitors: why, how, and where is the technology? *Journal of Power Sources* **91**, 37.

[42]**Kotz, R. and M. Carlen** 2000. Principles and applications of electrochemical capacitors.Electrochimica Acta, **45**, 2483.

[43]**Sezgin S.,** 2007. Electropolymerization of N-Pyrrole, N-Phenyl Pyrrole, (1-(4-Methoxyphenyl)1-H-Pyrrole on Carbon Fiber Micro Electrodes, Characterizations and Biosensor Applications**,** *MSc Thesis,* İ.T.Ü. Instute of Science and Technology, İstanbul.

[44]**Shirale, D.J., Gade, V.K., Gaikwad, P.D., Kharat, H.J., Kakde, K.P., Savale, P.A., Hussaini, S.S., Dhumane, N.R., Shirsat, M.D.,** 2006. The influence of electrochemical process parameters on the conductivity of poly(N-methylpyrrole) films by galvanostatic method, *Journal of Materials Letters*, **60**, 1407.

[45]**Zheng, J. P., Cygon, P., Jow, T. R.,** 1995. Ideal capacitive behavior of hydrous manganese oxide prepared by anodic deposition *Journal of Electrochem. Soc.,* **142**, 2699.

[46]**Saraç, A. S.,** Polymer Science and Technology Booklet, Cyclic Voltammetry.

[47]**Saraç, A. S., Serantoni, M., Tofail, S. A. M. , Cunnane, V. J**., 2004. Morphologial and spectroscopic analyses of poly [N-Vinylcarbazole-co-vinylbenzenesulfonic acid] copolymer electrografted on carbon fiber: the effect of current density, *Applied Surface Science*, **229**, 13.

[48]**Sarac, A. S., Serantoni , M., Tofail, S. A. M. Cunnane, V. Mcmonagle, J, B.,** Characterization of nanosize thin films of electrografted N-inylcarbazole copolymers (P[NVCz –co - VBSA] and P[NVCz-co-3-MhTh]) onto carbon fiber AFM, XPS, and Raman Spectroscopy, *Applied Surface Science*, **243**, 183.

[49]**Sonmez, G. and , Sarac, A. S.,** 2003. Structural study of pyrrole-EDOT copolymers on carbon fiber micro-electrodes, *Synthetic Metals*, **135**, 459-460.

[50]**Jamal M., Sarac, A. S., and Magner**, **E.**, 2004. Conductive copolymermodified carbon fibre microelectrode: electrode characterization and electrochemical detection of P-aminophenol, Sensors and actuators B-Chemical, **97**, 59-66.

[51]**Serantoni, M., Sarac, A. S., and Suddon, D.,** 2005. FIB-SIMS investigation of carbazole-based polymer and coploymers electrocoated onto carbon fibers and an AFM morphological study, *Surface&Coatings Technology,* **194**, 36-41

[52]**Bard, A.J; Faulkner, L. R.** Electrochemicel Methods; Wiley&Sons: New York, 2001; Chapters 3, 5, 7, 10, 13.

[53]**Schmickler W**. Interfacial Electrochemistry; Oxford University Pres: Oxford, 1996.

[54]**Parsons, R.** 1990. The electrical double layer: recent experimental and theoretical developments *Chemical. Reviews*. **90**, 813.

[55]**Randles, J. E. B.** 1948.Use of Electrically Excited Oxygen for the Low Temperature Decomposition of Organic Substances, *Trans. Faraday Faraday Soc*., **44**, 327.

[56]**Pankaj, S.,** 1997. Preparation, characterization and applications of ultrathin cellulose acetate Langmuir - Blodgett films, *Journal of Electroanalytical Chemistry*, **69**, 1662.

[57]**Macdonald, J. R.** Impedance Spectroscopy; Wiley- Interscience: New York 1987.

[58]**Sluyters-Rehback, M.; Sluyters, J. H**. 1970. *In Electroanalytical Chemistry*; Bard, A. J., Ed.; Marcel Dekker; New York, Vol. 4.

[59]**De Levie, R.; Husovsky, A. A.** 1969. *Journal of Electroanalytical Chemistry*. **20,** 181.

[60]**Armstrong, R. D.; Henderson, M.J**. 1972. The nature of o xide films on Tungsten in acidic and alkaline solutions, *Journal of Electroanalytical Chemistry*, **40**, 121.

[61]**Armstorng, R. D.; Race, W. P.; Thirsk, H. R.** 1974. Possibility of utilizing electrochemical techniques for the evaluation of the content of organic impurities in water *Electrochim. Acta*, **19**, 215

[62]**Su-Moon Park,Jung Suk Yoo**, 2003. Analytical Chemistry, **1**,455

[63]**R. Carpick page,** Wisconsin University, Madison, WI.
http://mandm.engr.wisc.edu/faculty_pages/carpick/research.htm

[64]**A. L Barabási,, H. E. Stanley**. Fractal concepts in surface growth. Cambridge University press, Great Britain, 1995.

[65]**G. Binnig, C.F. Quate, Ch. Geber,** 1986. Atomic Force Microscope,Phys. Rev. Letters, **56,** 90

[66]**Paul E. West**,2004. An Introduction to Atomic Force Microscopy ,Pacific Nanotech Press.

[67]**K. Zong, L. Madrigal, L. Groenendaal, J. R. Reynolds,** Chem. Commun. 2002, 2498.

[68]**B. Sankaran, J. R. Reynolds,** Macromolecules 30 (1997) 2582.

[69]**G. Rauchschwalbe, F. Jonas,** EP 1142888, (10.10.2001), CA 135 (2001) 289187e.

[70]**H. Randriamahazaka , C. Plesse, D. Teyssé, C. Chevrot,** 2003. *Electrochemistry Communications*, **5**, 613.

[71]**P. Fiordiponti, G. Pistoia**, 1989. An impedance study of polyaniline films in aqueous and organic solutions, *Electrochimica Acta*, **34**, 215.

[72]**Sipahi M. , Parlak E.A. , Gul A. , Ekinci E., Ferhat M., Sarac A. S.** , 2007. Electrochemical impedance study of polyaniline electrocoated porous carbon foam , *Progress in Organic Coatings*, (AIP)

[73]**C. L. Gaupp, D. M. Welsh und J. R. Reynolds,** 2002. Poly(ProDOT-Et_2): A High-Contrast, High-Coloration Efficiency Electrochromic Polymer *Macromolecules Rapid Communications*. **23**, 885-889

[74]**S. Fletcher**, 1992. Electrical model circuit that reproduces the behaviour of conducting polymer electrodes in electrolyte solutions.*Journal of Electroanalytical Chemistry,* **337,** 127.

6. BIOGRAPHY

Can Metehan Turhan was born in Edirne in 1982. After finishing primary, secondary and high school in Lüleburgaz, he obtained her B.Sc. in Chemistry from Eskişehir Osmangazi University in 2005.

He started his M.Sc. in Polymer Science and Technology at Istanbul Technical University in 2006.

His research interests are mainly focus on polyelectrolyte systems, surface chemistry, scanning probe systems, nanotechnology, materials science, electrochemistry; electrochemical impedance spectroscopy, conducting polymers and supercapacitors.

He has been working as a TUBİTAK scholar in Polymer Science and Technology Department of Istanbul Technical University under supervision of Prof. Dr. A. Sezai SARAÇ since January 2006.